

The International Journal of Robotics Research

<http://ijr.sagepub.com/>

On-line estimation of variable stiffness in flexible robot joints

Fabrizio Flacco, Alessandro De Luca, Irene Sardellitti and Nikos G Tsagarakis

The International Journal of Robotics Research 2012 31: 1556 originally published online 29 October 2012

DOI: 10.1177/0278364912461813

The online version of this article can be found at:

<http://ijr.sagepub.com/content/31/13/1556>

Published by:



<http://www.sagepublications.com>

On behalf of:



Multimedia Archives

Additional services and information for *The International Journal of Robotics Research* can be found at:

Email Alerts: <http://ijr.sagepub.com/cgi/alerts>

Subscriptions: <http://ijr.sagepub.com/subscriptions>

Reprints: <http://www.sagepub.com/journalsReprints.nav>

Permissions: <http://www.sagepub.com/journalsPermissions.nav>

Citations: <http://ijr.sagepub.com/content/31/13/1556.refs.html>

>> [Version of Record](#) - Nov 30, 2012

[OnlineFirst Version of Record](#) - Oct 29, 2012

[What is This?](#)

On-line estimation of variable stiffness in flexible robot joints

Fabrizio Flacco¹, Alessandro De Luca¹, Irene Sardellitti² and Nikos G Tsagarakis²

Abstract

Variable stiffness actuators (VSAs) are currently explored as a new actuation approach to increase safety in physical human–robot interaction (pHRI) and improve dynamic performance of robots. For control purposes, accurate knowledge is needed of the varying stiffness at the robot joints, which is not directly measurable, nonlinearly depending on transmission deformation, and uncertain to be modeled. We address the online estimation of transmission stiffness in robots driven by VSAs in antagonistic or serial configuration, without the need for joint torque sensing. The two-stage approach combines (i) a residual-based estimator of the torque at the flexible transmission, and (ii) a recursive least squares stiffness estimator based on a parametric model. Further design refinements guarantee a robust behavior in the lack of velocity measures and in poor excitation conditions. The proposed stiffness estimation can be easily extended to multi-degree-of-freedom (multi-DOF) robots in a decentralized way, using only local motor and link position measurements. The method is tested through extensive simulations on the VSA-II device of the University of Pisa and on the Actuator with Adjustable Stiffness (AwAS) of IIT. Experiments on the AwAS platform validate the approach.

Keywords

Robots with flexible joints, variable stiffness, on-line estimation, residuals, recursive least squares

1. Introduction

Flexibility in the robot transmissions has been considered in the past as an undesired behavior, being a source of static and dynamic inaccuracy at the robot end-effector level and potentially leading to control instability problems (De Luca and Book, 2008). Recent research in physical human–robot interaction (pHRI) has shown that introduction of compliance in the robot structure may help in reducing the risk of injuries due to accidental human–robot collisions (Bicchi and Tonietti, 2004; Haddadin et al., 2007; Bicchi et al., 2008b), with compliant elements absorbing part of the impact energy (Ikuta et al., 2003). On the other hand, the capability of storing potential energy in the compliant actuators and releasing it in due time may improve the execution of heavily dynamic tasks, such as robotic hammering of nails (Garabini et al., 2011) or kicking/throwing an object as far as possible (Haddadin et al., 2009).

A compliant robot behavior may be achieved through the use of flexible mechanical components, or via feedback control, or typically by combining the two (De Santis et al., 2008). In view of the intrinsic limited bandwidth of control algorithms, a convenient way to introduce mechanical compliance in a robot arm is to design

on purpose flexible joints/transmissions. An inertial decoupling is then obtained between the heavier motors and the usually lightweight links, limiting the energy transfer from the robot to a human in the case of impacts. This is a relevant feature of manipulators such as the Barrett WAM (Salisbury et al., 1988) or the DRL/KUKA LWR series (Hirzinger et al., 2001). Transmission flexibility in these robots is due to the use of harmonic drives or cables, and can be reasonably considered as a linear effect (joint elasticity). The same is true also in robotic structures based on series elastic actuation (SEA) (Pratt and Williamson, 1995). Robots with non-negligible joint elasticity can still perform very accurate free motion as well as stable compliant interaction tasks thanks to a nonlinear control design, see, e.g.,

¹Dipartimento di Ingegneria Informatica, Automatica e Gestionale, Università di Roma “La Sapienza”, Roma, Italy

²Advanced Robotics Lab, Istituto Italiano di Tecnologia, Genova, Italy

Corresponding author:

Alessandro De Luca, Dipartimento di Ingegneria Informatica, Automatica e Gestionale, Università di Roma “La Sapienza”, Via Ariosto 25, 00185 Roma, Italy.

Email: deluca@dis.uniroma1.it

Spong (1987), De Luca and Lucibello (1998), De Luca et al. (2005), and Kugi et al. (2008), as long as a reliable dynamic model (including joint stiffness) is available. Since the joint stiffness is assumed to be constant in this case, its identification by offline static calibration procedures is feasible.

It should be noted that a fixed mechanical stiffness at the joints allows only a fixed Cartesian compliance for a given robot configuration. Modification of this compliance requires the presence of kinematic redundancy (changing the robot configuration at a given robot end-effector pose) and/or the tuning of the positional gains in a feedback control law (see Petit and Albu-Schäffer, 2011). In addition, the risks of (human or robot) damages due to collisions are reduced when the joints are very compliant, whereas high motion performance with fast acceleration transients requires the transmissions to be stiffer, so as to transfer efficiently the kinetic energy from the motors to the links. This is the outcome of the safe brachistochrone analysis presented in Bicchi and Tonietti (2004).

The above considerations have led in the recent years to the development of variable stiffness actuation (VSA) for robot arms (and legs), where the joint stiffness can be varied on the fly during the commanded motion. This is obtained by using two actuators and flexible transmissions that have nonlinear torque/deformation characteristic. Several different realization of the VSA principle have been investigated, exploiting pneumatic muscles or electrical motors as actuation devices (Van Ham et al., 2009), but most designs can be grouped in two main categories. The first arranges the two actuators and the associated nonlinear transmissions in an agonistic–antagonist configuration (Migliore et al., 2005; Tonietti et al., 2005; Schiavi et al., 2008). In this bio-inspired design, motion and stiffness actuation have a strong dynamic coupling. The second category of VSA, the so-called serial configuration, is conceptually different: there is a single flexible transmission driven by a primary motor for controlling the link motion, while a secondary, typically smaller motor controls separately the actual stiffness of the transmission (Van Ham et al., 2007; Choi et al., 2008; Wolf and Hirzinger, 2008; Ikegami et al., 2009; Jafari et al., 2010; Tsagarakis et al., 2011).

In parallel to the development of VSA devices, control laws have been investigated that are able to assign a desired behavior to both joint stiffness and link motion. Classical PD with feedforward compensation or PID laws can be designed for regulating both the position and the stiffness to constant values, in the absence (Tonietti et al., 2005) or presence (De Luca and Flacco, 2010) of gravity. The interplay between VSA design and the possibility of regulating the output stiffness of the device without changing the stored potential energy in the system has been studied by Visser et al. (2011) following a port-Hamiltonian approach. For the simultaneous tracking of smooth stiffness/motion trajectories, a gain scheduling method, improved in robustness through LQR, has been proposed by Sardellitti et al.

(2012). For the same problem, a nonlinear decoupling and exact linearizing state feedback law was introduced by De Luca et al. (2009) for the VSA-II device developed by the University of Pisa, and generalized to any multi-degree-of-freedom (multi-DOF) robot driven by antagonistic VSAs in Palli et al. (2008). This control law has the best possible nominal performance, but requires also the evaluation of the first and second derivatives of the stiffness with respect to the deformation variables.

All of the above control schemes need an accurate knowledge of the nonlinear stiffness of the VSA. However, there are no sensors available for a direct measure of the varying stiffness, in particular online (i.e. during dynamic robot operation). The device stiffness is usually computed from position and/or joint torque sensor data, based on a nominal mathematical model. This is especially critical for VSA-based manipulators since:

- (i) the stiffness characteristic profile is intrinsically nonlinear;
- (ii) the mathematical model can be a complex function of the deformation of the transmissions, subject to kinematic and dynamic uncertainties;
- (iii) the stiffness is a variable parameter that should be set explicitly under control.

The last issue implies an intrinsic weakness for any feedback control scheme, with or without a stiffness estimation procedure. As a matter of fact, in the absence of a direct measure of the controlled (stiffness) output, a control law can at best assign the desired reference behavior to the nominal output (or to the estimated output), but not necessarily to the actual one. Therefore, the robustness of an estimation method with respect to perturbations is particularly desired in such cases.

We should also remark that an online estimation problem is addressed. Conventional offline procedures of stiffness estimation may be set up using quasi-static measurements of transmission deflection in response to known or measured applied torques. However, this may fail to provide ‘ground truth’ values of stiffness when the actuation device is in actual operation. By tackling the estimation problem on line, it is possible to gather information on the transmission stiffness in dynamic conditions for the actuator, thus bringing into play higher frequency effects, e.g. due to sudden and large accelerations, or very different operating conditions, e.g. with or without payload.

1.1. Literature review

While many papers have dealt with stiffness estimation in contact situations between the end-effector of a rigid robot and the environment or a human (Diolaiti et al., 2005; Verscheure et al., 2009; Ludvig and Kearney, 2009; Coutinho and Cortesao, 2010), less work has been devoted in the past to the estimation of variable, nonlinear stiffness of flexible joints.

With the recent diffusion of several new devices, there is an interest in the development of reliable on-line stiffness estimation methods for VSAs.¹ Grioli and Bicchi (2010) proposed a dynamic observer for a simple variable stiffness model that achieves ultimately bounded error in stiffness estimation. Knowledge of the applied external torque and of its time derivative is assumed and (multiple) numerical differentiation of the measured position is needed. Serio et al. (2011) developed and complemented this approach with an extended Kalman filter (EKF) in order to estimate simultaneously the transmission stiffness as well as the (link) inertia and damping. This extended method requires a joint torque sensor and uses again numerical differentiation of the measured (flexibility) torque and/or time derivatives of position measurements, leading to high sensitivity to noise. Moreover, an interaction loop is present between the stiffness observer and the EKF inertia/damping estimator, producing poor excitation conditions. These drawbacks have been partly alleviated in Grioli and Bicchi (2011), by resorting to a parametric model of the torque/deformation characteristic of the transmission,² which eliminates the need for multiple numerical differentiations of signals. However, the stiffness estimator of Grioli and Bicchi (2011) relies still on the use of a joint torque sensor for measuring the flexibility torque of the transmission. Differentiation of this measurement can be avoided by using a prediction error on the estimated transmission torque, but in this case the convergence of the model parameters is slowed down.

One of the difficulties encountered by the authors of these works was due to the desire to obtain a stiffness estimate in the least invasive way for the actuation device, i.e. by operating from the link side of the transmissions. In turn, the need for extra sensing and signal derivatives can be easily avoided when the problem is attacked from the motor side. Following this line of thought, we have developed in Flacco and De Luca (2011a) an initial set of stiffness estimators that does not need joint torque sensing and can be applied in a similar way to a single flexible transmission or to double flexible transmissions in antagonist arrangement. The information given by joint torque sensors is replaced by the use of (residual) estimators monitoring the evolution of the momentum associated with each motor dynamics, an idea originally developed in the context of actuator fault detection for mechanical/robotic systems (De Luca and Mattone, 2003) and later applied also to robot collision detection problems (De Luca et al., 2006). The residual provides a low-pass filtered version of the unmeasured torque across the flexible transmission. From this, stiffness was estimated in two alternative ways: using a black-box regressor, without any assumed model for the unknown quantity; or applying a least squares method in batch mode, based on a model where the unknown coefficients appear in a nonlinear way. The first variant can work on line, requiring minimal a priori information. However, only point-wise stiffness estimation is provided so that the method is not useful when differential functional expressions of the identified stiffness are

needed, as in the decoupling and linearizing control of VSA devices of (De Luca et al., 2009). The second variant produces better results, but it was not intended for a real-time implementation.

1.2. Paper contributions and organization

In this paper, we present a unified approach to the on-line stiffness estimation problem, consolidating and expanding the results of our more recent works (Flacco and De Luca, 2011b; Flacco et al., 2011). The method consists of two stages. In the first stage, a residual-based estimator of the flexibility torque is designed for a single nonlinear transmission without using joint torque sensing. In the second stage, we resort to a recursive least squares (RLS) estimator based on a linearly parameterized model of the transmission torque/deformation characteristic. As a byproduct, this allows to generate a functional estimation of the stiffness, from which further differential expressions can be directly obtained. Starting from this basic result, minor modifications are needed to address the problem of estimating the stiffness of VSA devices both in antagonistic and in serial configurations. In fact, the two-stage estimation is fully designed on the motor side of a robot transmission, leading to three relevant features:

- (i) only motor and link position measurements and motor dynamic parameters are used;
- (ii) the approach can be replicated as needed for each flexible transmission that is affecting the device stiffness of a (antagonistic or serial) VSA;
- (iii) the same method can be implemented for multi-DOF VSA-driven robots in a fully decentralized way.

In order to achieve a more robust estimation, the first stage is refined by using a suitably modified version of the discrete-time kinematic Kalman filter of Jeon and Tomizuka (2007). This avoids the need for numerical differentiation of motor position measurements when computing the residuals and handles efficiently also encoder quantization errors—a potential problem in implementations. Moreover, the performance of the RLS algorithm used in the second stage is enhanced using a technique proposed by Bitanti et al. (1990), which ensures parameter convergence or at least stability of the stiffness estimation also in conditions of poor excitation, e.g. when the flexible transmissions undergo only relatively small deformations.

The paper is organized as follows. The dynamic modeling framework is introduced in Section 2, starting from a single flexible transmission and covering both antagonistic and serial VSA devices. In Section 3, we present the two-stage stiffness estimation method for a nonlinear flexible transmission, and then directly also for a VSA with antagonistic configuration of two motors using such transmissions. The modifications needed for estimating the stiffness of a VSA in serial configuration are presented in Section 4. In Section 5, the problem of lack of sufficient excitation is

addressed. Section 6 is devoted to the evaluation of the proposed stiffness estimation method through realistic simulations. We first consider two paradigmatic single-DOF VSA case studies: the VSA-II antagonistic device, developed at the University of Pisa; and the Actuator with Adjustable Stiffness (AwAS) serial device, developed at IIT. We report then the results obtained for a two-DOF planar manipulator driven by VSA-II actuators and moving in the vertical plane. Guidelines for choosing the parameters for robust performance are given in Section 7. Finally, experimental results obtained on the AwAS platform (Jafari et al., 2010) are presented in Section 8, validating the stiffness estimation method also with respect to the alternative use of the joint torque sensor available on this device. A discussion on the use of the proposed online stiffness estimation in control laws and on possible extensions concludes the paper.

With respect to our conference works (Flacco and De Luca, 2011b; Flacco et al., 2011), the new contributions of this paper include: a thorough evaluation of the method by realistic simulations both on the VSA-II (Section 6.1) and AwAS (Section 6.2) devices, using more demanding commanded motions and showing convergence of the estimated model parameters; verification of the similar performance obtained in the case of a two-DOF VSA-based robot (Section 6.3); the guidelines for choosing the gains and parameters involved in the method, with a sensitivity analysis with respect to the resolution of position encoders (Section 7); a more complete presentation of the experimental results on the AwAS, illustrating in particular the convergence behavior of the coefficients in the used parametric model and a further validation of the estimation method on new experimental data.

2. Dynamic modeling

Flexible joints are characterized by a deformable transmission that connects the driving actuator to the driven link. In the following we focus only on actuation provided by electrical motors, even if many of the concepts can be extended also to pneumatic actuators.

2.1. Single flexible transmission

The deformation ϕ of the transmission is the difference between the link angle q and the motor angle θ ($\phi = q - \theta$). The latter is possibly reflected through a reduction gear with ratio $\gamma \geq 1$, i.e. $\dot{\theta} = \dot{\theta}_m/\gamma$, where θ_m is the position of the motor as measured by an encoder mounted on its axis.³ Let $U_e(\phi) \geq 0$ be the potential energy associated with the deformation ϕ , with $U_e(\phi) = 0$ if and only if $\phi = 0$. The torque transferred from the motor to the link through the flexible transmission is given by $\tau_e(\phi) = \partial U_e(\phi)/\partial \phi$, which is in general a nonlinear function of ϕ . To distinguish it from the motor torque τ , throughout the paper we call $\tau_e(\phi)$ the flexibility torque. We assume that

$$\tau_e(0) = 0, \tag{1}$$

i.e. no torque is provided through the undeformed transmission.⁴ In many cases, the additional condition

$$\tau_e(-\phi) = -\tau_e(\phi), \quad \forall \phi \tag{2}$$

holds, namely when the transmission has the same behavior in compression and extension.

When a single motor drives through a (nonlinear) flexible transmission a rigid link, possibly subject to gravity, the dynamic model takes the form

$$M\ddot{q} + D_q\dot{q} + \tau_e(\phi) + g(q) = \tau_{\text{ext}} \tag{3}$$

$$B\ddot{\theta} + D_\theta\dot{\theta} - \tau_e(\phi) = \tau, \tag{4}$$

where $M > 0$ and $B = B_m\gamma^2 > 0$ are the link inertia and the reflected motor inertia (with the rotor having inertia B_m), $D_q \geq 0$ and $D_\theta = D_{\theta,m}\gamma^2 \geq 0$ are the viscous friction coefficients at the two sides of the transmission, τ is the motor control torque reflected through the gear ratio ($\tau = \tau_m\gamma$, being τ_m the motor torque on its output axis), and $g(q)$ and τ_{ext} are, respectively, the gravity and the environment/disturbance torques acting on the link.

The stiffness of the transmission is defined as the rate of variation of the torque $\tau_e(\phi)$ with respect to the deformation ϕ ,

$$\sigma(\phi) = \frac{\partial \tau_e(\phi)}{\partial \phi} > 0. \tag{5}$$

While slightly different definitions of stiffness can be found in the literature (see, e.g., Ozawa and Kobayashi, 2002; Grioli and Bicchi, 2011), we consider in (5) the internal stiffness of the transmission/flexible joint, usually called passive stiffness. Passive stiffness refers thus to the torque needed to deform the transmission. In the absence of gravity ($g(q) \equiv 0$), the passive stiffness coincides with the external stiffness

$$\sigma_{\text{ext}}(\phi) = \frac{\partial \tau_{\text{ext}}}{\partial q} = \frac{\partial \tau_{\text{ext}}}{\partial \phi} = \left(\frac{\partial \phi}{\partial \tau_{\text{ext}}} \right)^{-1}, \tag{6}$$

which is the inverse of the compliance of the joint, i.e. the rate of deformation of the transmission in response to external torques τ_{ext} applied to the link in static conditions (with the motor position θ kept fixed). Such a compliance can be evaluated experimentally.

The basic model (3)–(4) can be modified rather directly to express the dynamics of an actuator with variable stiffness. For this purpose, it is necessary to distinguish the cases of VSA in antagonistic or serial configurations,⁵ see Figure 1 and the definition of the variables therein.

2.2. Antagonistic VSA

An antagonistic VSA is characterized by two motors working in parallel and antagonistically connected to the driven link through nonlinear transmissions. Although different arrangements are possible, we consider here only the bidirectional one, see Bicchi et al. (2008a). Depending on

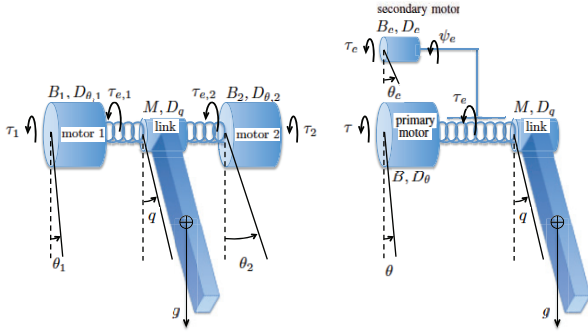


Fig. 1. Schematics of VSA in antagonistic (left) or serial (right) configurations driving a single link under gravity

the realization, the nonlinearity of the deformation/torque characteristic of the transmissions results either by the use of nonlinear (e.g. cubic or exponential) springs or by the arrangement of linear springs in a nonlinear kinematic mechanism. Representative devices in this class are the biologically inspired VSA (Migliore et al., 2005) and the VSA-II (Schiavi et al., 2008).

The two motor-transmission units are modeled with two similar equations of the form (4), where each motor-transmission undergoes a deformation $\phi_i = q - \theta_i$, for $i = 1, 2$. The dynamics of an antagonistic VSA is thus

$$M\ddot{q} + D_q\dot{q} + \tau_{e,t}(\phi) + g(q) = \tau_{\text{ext}} \quad (7)$$

$$B_i\ddot{\theta}_i + D_{\theta,i}\dot{\theta}_i - \tau_{e,i}(\phi_i) = \tau_i, \quad i = 1, 2. \quad (8)$$

In this case, the total flexibility torque transmitted to the driven link and the associated (total) device stiffness are given by

$$\tau_{e,t} = \tau_{e,1}(\phi_1) + \tau_{e,2}(\phi_2) \quad (9)$$

and

$$\sigma_t(\phi) = \sigma_1(\phi_1) + \sigma_2(\phi_2), \quad (10)$$

where

$$\sigma_i(\phi_i) = \frac{\partial \tau_{e,i}(\phi_i)}{\partial \phi_i} > 0, \quad i = 1, 2, \quad (11)$$

are the local stiffnesses of the two transmissions and $\phi = (\phi_1 \ \phi_2)^T$. We stress the separability of the functions (9) and (10), whereas in general $\phi_1 \neq \phi_2$. Most of the time the two motor-transmission units are identical (perfect symmetry). However, our later developments apply directly also to the general case.

2.3. Serial VSA

A serial VSA consists of a primary motor, used to command the link motion through the flexible transmission, and of a secondary motor, used to modify the stiffness of the transmission by changing the operating point on its characteristic (or, equivalently, by shaping the potential energy associated with the deformation). Representative devices in this class are the MACCEPA (Van Ham et al., 2007), the

DLR VS-joint (Wolf and Hirzinger, 2008), and the AwAS (Jafari et al., 2010).

The angular position of the secondary motor (called also set-point variable), as reflected through a reduction gear with ratio $\gamma_c \geq 1$, will be denoted by θ_c . In this case, the dynamic model takes the form

$$\begin{aligned} M\ddot{q} + D_q\dot{q} + \tau_c(\theta_c, \phi) + g(q) &= \tau_{\text{ext}}, \\ B\ddot{\theta} + D_\theta\dot{\theta} - \tau_e(\theta_c, \phi) &= \tau, \\ B_c\ddot{\theta}_c + D_{\theta,c}\dot{\theta}_c + \psi_e(\theta_c, \phi) &= \tau_c, \end{aligned} \quad (12)$$

where, together with the notation inherited from (3)–(4), $B_c = B_{m,c}\gamma_c^2 > 0$ and $D_{\theta,c} = D_{\theta m,c}\gamma_c^2 \geq 0$ are, respectively, the reflected inertia and viscous friction coefficient of the secondary motor, and τ_c is its reflected torque ($\tau_c = \tau_{m,c}\gamma_c$). The function $\psi_e(\theta_c, \phi)$ is the coupled flexibility torque, representing how the transmission deformation reacts on the secondary motor as a function of the set-point variable. Actually, this is an undesirable dynamic coupling behavior and mechanical solutions that minimize this effect are usually chosen. The device stiffness is defined in this case as

$$\sigma(\theta_c, \phi) = \frac{\partial \tau_e(\theta_c, \phi)}{\partial \phi}, \quad (13)$$

since the coupled flexibility torque plays no role in this regard.

2.4. Multi-DOF VSA-driven robots

A general dynamic model of a N -DOF manipulator driven by VSA can be written by compounding the robot link dynamics with the proper motor equations introduced in the previous sections. Under an assumption similar to that used by Spong (1987) for modeling robots with elastic joints of constant stiffness, i.e. that the rotational kinetic energy of the rotors of the two motors at each joint is due only to their own spinning, the dynamic model of a robot with antagonistic VSA takes the form

$$\begin{aligned} M(q)\ddot{q} + C(q, \dot{q})\dot{q} + D_q\dot{q} \\ + (\tau_{e,1}(\phi) + \tau_{e,2}(\phi)) + g(q) &= \tau_{\text{ext}}, \\ B_1\ddot{\theta}_1 + D_1\dot{\theta}_1 - \tau_{e,1}(\phi) &= \tau_1, \\ B_2\ddot{\theta}_2 + D_2\dot{\theta}_2 - \tau_{e,2}(\phi) &= \tau_2, \end{aligned} \quad (14)$$

where $q \in \mathbb{R}^N$, $\theta \in \mathbb{R}^N$, $\phi = q - \theta$, $M > 0$ is link inertia matrix, C is the factorization matrix of the Coriolis and centrifugal terms, $D_q \geq 0$ is the (diagonal) viscous friction matrix on the link sides, and g is the gravity vector term. Moreover, for $j = 1, 2$, the matrices B_j and D_j of motor inertias and damping are diagonal, while the dependence of the flexibility torque vectors $\tau_{e,j}$ on ϕ is component-wise separable (the k th component depends only on ϕ_k). A similar model can be written for the serial VSA case.

3. Stiffness estimation for antagonistic VSA

With reference to the models (3)–(4), (7)–(8), and (12) for a single actuated flexible transmission, for an antagonistic VSA, and for a serial VSA, respectively, our goal is to estimate online the varying device stiffness in each case. We do this without the need for additional (e.g. joint torque) sensors beyond the encoders placed at the link and motor(s) sides, nor of time derivatives of these position measurements. From the structure of $\sigma_i(\phi)$ in (10) and of the motor equations in (8), as well as from the dependence of $\sigma(\theta_c, \phi)$ in (13) and the primary motor equation in (12), it is easy to see that a unified approach can be followed by addressing first the estimation of a single transmission stiffness on the motor side, and then extending the method to the other cases. The same argument applies also for the multi-DOF robot case in Equation (14), where we take advantage of the decentralized structure of the motor equations.

The estimation is performed in two stages, estimating the flexibility torque $\tau_e(\phi)$ with a residual-based technique, and using then this result to estimate online the stiffness $\sigma(\phi)$ with a RLS algorithm based on a parametric model.

3.1. Residual for estimation of the flexibility torque

With reference to Equations (3)–(4), a residual signal can be generated that provides a filtered version of the unmeasured flexibility torque $\tau_e(\phi)$. Denoting by $p = B\dot{\theta}$ the generalized momentum of the motor, the residual is defined as

$$r_e = K_I \left(p + D_\theta \theta - \int_0^t (\tau + r_e) ds \right), \quad (15)$$

where $K_I > 0$ is a free design parameter. From Equation (4), it is easy to check that the residual r_e satisfies

$$\dot{r}_e = K_I (\tau_e(\phi) - r_e), \quad (16)$$

resulting in a first-order, stable filter of the unknown flexibility torque. A discrete-time implementation of the residual $r_e(k) = r_e(t_k)$ at $t = t_k = kT$ is obtained using Tustin rule in (15), yielding

$$\begin{aligned} I_\tau(k) &= I_\tau(k-1) + \frac{\tau(k) + \tau(k-1)}{2} T, \\ \bar{r}(k) &= K_I (B\dot{\theta}(k) + D_\theta \theta(k) - I_\tau(k)), \\ r_e(k) &= \frac{2 - TK_I}{2 + TK_I} r_e(k-1) + \frac{2(\bar{r}(k) - \bar{r}(k-1))}{2 + TK_I}, \end{aligned} \quad (17)$$

where T is the sampling time.

It should be noted that the flexibility torque is estimated using only the motor parameters B and D_θ , which can be taken from the motor data sheet. The motor torque τ is obtained from the known commanded current and the current/torque gain of the motor.⁶ The motor position θ is measured by an encoder and its velocity $\dot{\theta}$ (needed in p) is obtained numerically.

However, time discretization of signals and the presence of encoder quantization may introduce excessive noise when computing the motor angular velocity by numerical differentiation. A possible solution that avoids the use of motor velocity is to define a second-order residual, along the line proposed by Flacco and De Luca (2011a). This approach was not pursued further since it introduces a two-step delay in the estimation and an additional need of tuning the residual gains.

We developed instead a modified kinematic Kalman filter (MKKF), a novel solution inspired by the work of Jeon and Tomizuka (2007). Let x be an angular position and \dot{x} the associated angular velocity. In order to estimate $\xi(k) = \xi(t_k) = (x(k) \dot{x}(k))^T$ with a kinematic Kalman filter, the following system is considered

$$\xi(k) = \begin{pmatrix} 1 & T \\ 0 & 1 \end{pmatrix} \xi(k-1) + \mu(k) \quad (18)$$

$$z(k) = (1 \ 0) \xi(k) + v(k), \quad (19)$$

where $z(k)$ is the noisy sampled measure (the encoder angle in our case) and $\mu(k)$ and $v(k)$ are discrete-time realizations of zero mean Gaussian noises having, respectively, covariance matrix Q and variance R . In the state equation (18), acceleration is not considered and μ represents also the noise due to this absence. By defining $\Gamma = (T^2/2 \ T)^T$, the covariance matrix of μ is $Q = V_a \Gamma \Gamma^T$, where V_a is the variance associated with the state. While the variance R of the measures is usually set to a constant value, in the proposed MKKF we choose it as a function of the estimated velocity, since the noise due to encoder quantization is significant at low speed and negligible at high speed. In particular, we used

$$R(k) = \frac{V_{\max} - V_{\min}}{1 + e^{(|\dot{x}(k)|w_s - 1)\alpha}} + V_{\min}, \quad (20)$$

where V_{\max} and V_{\min} are the maximum and minimum variances considered, $w_s = (2\pi/\Delta)/T$, being $2\pi/\Delta$ the encoder resolution, and α is a shaping factor. The resulting effects of this choices are discussed in Section 6. In the rest of the paper, whenever we refer to an angular position and/or velocity, we consider their values as obtained from the MKKF system (18)–(19).

3.2. Stiffness estimation based on RLS

In this second stage, the flexibility torque $\tau_e(\phi)$ is approximated by a parametric model $f(\phi, \alpha)$, typically chosen as linear in the unknown n -dimensional parameter vector α , which is identified using a standard RLS algorithm (see, e.g., Johnson, 1988). From computed or measured data, we set thus the relationship

$$\widehat{\tau}_e(\phi(k)) = f(\phi(k), \alpha) = F^T(k) \alpha, \quad (21)$$

where $\phi(k)$ is the deformation measured at time $t_k = kT$ and $\widehat{\tau}_e(\phi(k))$ may be either the measured flexibility torque,

if a joint torque sensor is available, or otherwise its estimate given by the residual $r_e(k)$ in Equation (17). The n -dimensional row vector \mathbf{F}^T is the Jacobian of $f(\phi, \boldsymbol{\alpha})$ with respect to parameter $\boldsymbol{\alpha}$.

For the online minimization of the sum of the squares of the estimation errors up to time t_k

$$E(k) = \sum_{i=1}^k \left(\widehat{\tau}_e(\phi(i)) - \mathbf{F}^T(i) \boldsymbol{\alpha} \right)^2, \quad (22)$$

the RLS algorithm provides the current estimate $\widehat{\boldsymbol{\alpha}}(k)$ as follows:

$$\begin{aligned} \epsilon(k) &= \widehat{\tau}_e(\phi(k)) - \mathbf{F}^T(k) \widehat{\boldsymbol{\alpha}}(k-1), \\ \rho(k) &= \mathbf{F}^T(k) \mathbf{P}(k-1) \mathbf{F}(k), \\ \mathbf{K}(k) &= \frac{\mathbf{P}(k-1) \mathbf{F}(k)}{1 + \rho(k)}, \\ \widehat{\boldsymbol{\alpha}}(k) &= \widehat{\boldsymbol{\alpha}}(k-1) + \mathbf{K}(k) \epsilon(k), \\ \mathbf{P}(k) &= \mathbf{P}(k-1) - \mathbf{K}(k) \mathbf{F}^T(k) \mathbf{P}(k-1). \end{aligned} \quad (23)$$

The algorithm is initialized with an a priori estimate $\widehat{\boldsymbol{\alpha}}(0)$ of the parameters and a symmetric (typically, diagonal) matrix $\mathbf{P}(0) > 0$. The previous estimation is updated based on the current error $\epsilon(k)$ between the residual/measure and the predicted flexibility torque of the transmission. Inside the algorithm (23), matrix \mathbf{P} plays the same role as the covariance matrix in a stochastic setting. The larger the covariance, the larger will be the update of the parameters. Therefore, the covariance matrix \mathbf{P} should be initialized with large values in case of poor a priori knowledge about the parameters. The elements of matrix \mathbf{P} typically decrease at each step and there will be no significant parameter updates when the updating factor becomes too small. We remark that the degree of the polynomial $f(\phi(k), \boldsymbol{\alpha})$ should be adequate for capturing the nonlinearity of the flexibility torque of the transmission. Otherwise, the RLS algorithm will not track efficiently the data or, even if it converges (\mathbf{P} is small), a non-negligible estimation error would result.

From the parametric model (21) that is currently being identified, stiffness estimation is directly obtained by analytic differentiation of $f(\phi(k), \widehat{\boldsymbol{\alpha}}(k))$ as

$$\widehat{\sigma}(\phi(k)) = \left(\frac{\partial \mathbf{F}(k)}{\partial \phi(k)} \right)^T \widehat{\boldsymbol{\alpha}}(k). \quad (24)$$

In the relationship (21),

$$f(\phi, \boldsymbol{\alpha}) = \mathbf{F}^T(\phi) \boldsymbol{\alpha} = \sum_{h=0}^{n-1} \alpha_h f_h(\phi), \quad (25)$$

the scalar parameters α_h , $h = 0, \dots, n-1$, weight linearly a set of basis functions $f_h(\phi)$ that are conveniently chosen as polynomial terms⁷ in ϕ . For a single (or a double antagonistic) flexible transmission, we take into account the assumption (1) on the flexibility torque. Moreover, when

the symmetric condition (2) holds true, we choose as basis functions in (25) only odd powers of ϕ up to the order $2n-1$,

$$f_h(\phi) = \phi^{2h+1}, \quad h = 0, \dots, n-1, \quad (26)$$

so that Equation (24) becomes

$$\widehat{\sigma}(\phi) = \sum_{h=0}^{n-1} (2h+1) \alpha_h \phi^{2h}. \quad (27)$$

In the same way, the derivative of the estimated stiffness with respect to the transmission deformation is obtained as

$$\frac{\partial \widehat{\sigma}(\phi)}{\partial \phi} = \sum_{h=1}^{n-1} (4h^2 + 2h) \alpha_h \phi^{2h-1}. \quad (28)$$

Equations (27) and (28), as well as a similar closed-form expression for the second derivative of the estimated stiffness, are needed in particular for the control laws proposed by De Luca et al. (2009) and De Luca and Flacco (2010).

The symmetric behavior (2) for the flexibility torque is quite common in VSA transmissions. In any event, if the estimator has to be used for a non-symmetric transmission and if we also wish to relax assumption (1), the only needed change is to use a polynomial basis with n terms containing all powers of ϕ up to a desired degree $n-1$, i.e.

$$f(\phi, \boldsymbol{\alpha}) = \sum_{h=0}^{n-1} \alpha_h f_h(\phi), \quad f_h(\phi) = \phi^h, \quad h = 0, \dots, n-1. \quad (29)$$

With this model, the coefficient α_0 associated with the zeroth order (constant and unitary) term in the basis will estimate the non-zero value $\tau_e(0)$.

For a VSA in antagonistic configuration, the stiffness of each transmission can be estimated separately and independently using the above method for a single flexible transmission. The total stiffness of the device will then be obtained from the relation (10). For a VSA in serial configuration, the method has to be slightly modified as illustrated in the next section.

4. Stiffness estimation for serial VSA

With reference to Figure 2, consider now a serial variable stiffness actuator modeled by Equations (12). The estimation of the flexibility torque $\tau_e(\theta_c, \phi)$ is obtained using as before Equation (17), since the dynamics at the primary motor side is identical and the dependence of τ_e also on θ_c plays no role in the definition of the residual. For stiffness estimation, the RLS algorithm (23) is used similarly. However, departing from the antagonistic VSA case (25), the linear parameterization of the flexibility torque should be introduced more carefully in order to take into account also the dependence on the position of the secondary motor.

The presence of the secondary motor does not affect the basic assumption (1), or

$$\tau_e(\theta_c, 0) = 0, \quad \forall \theta_c. \quad (30)$$

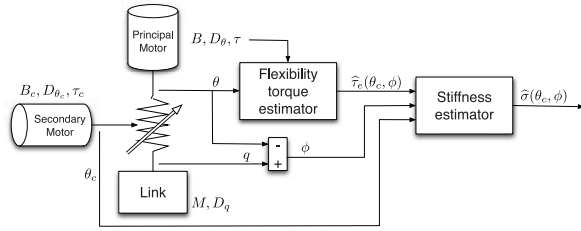


Fig. 2. Two-stage stiffness estimator for an actuator with variable stiffness in serial configuration

For the time being, let us further assume that the set-point variable θ_c of the secondary motor affects the shape of the flexibility torque in a separable way as

$$\tau_e(\theta_c, \phi) = \ell(\theta_c) h(\phi), \tag{31}$$

i.e. with a positive functional factor depending on θ_c that multiplies the flexibility term due to the deformation ϕ , and that the transmission displays a symmetric behavior of the flexibility torque with respect to the deformation (see also Equation (2))

$$\tau_e(\theta_c, -\phi) = -\tau_e(\theta_c, \phi), \quad \forall \theta_c, \phi, \tag{32}$$

similarly to the situation considered also in the antagonistic case.

As a consequence, in the parametric approximation of τ_e , we consider the following two polynomials for $h(\phi)$ and $\ell(\theta_c)$:

$$h(\phi, \alpha) = \sum_{i=0}^{n-1} \alpha_i \phi^{2i+1}, \quad \ell(\theta_c, \beta) = \sum_{j=0}^{m-1} \beta_j \theta_c^j. \tag{33}$$

Note that, for the sake of simplicity, we do not force positivity of the factor $\ell(\theta_c)$ since this would lead to the need to add constraints in the RLS algorithm without effective improvement of the estimate.

When combining Equations (31) and (33), it is apparent that for the estimation process we do not need a separate (and also quite non-trivial) estimation of the $n + m$ unknown parameters in vectors α and β , but we can linearly re-parameterize the problem in terms of a new vector η of the $n \cdot m$ scalar parameters

$$\eta_{ij} = \alpha_i \beta_j. \tag{34}$$

As a result, the parametric model f used for fitting τ_e will be chosen as

$$f(\theta_c, \phi, \eta) = \sum_{i=0}^{n-1} \sum_{j=0}^{m-1} \eta_{ij} \theta_c^j \phi^{2i+1} = \mathbf{F}^T(\theta_c, \phi) \boldsymbol{\eta}. \tag{35}$$

The Jacobian of $f(\theta_c, \phi, \eta)$ w.r.t. the new parameter vector η is given by the row vector

$$\mathbf{F}^T(\theta_c, \phi) = \begin{pmatrix} \phi & \phi^3 & \dots & \phi^{2n-1} \\ \theta_c \phi & \theta_c \phi^3 & \dots & \theta_c \phi^{2n-1} \\ \dots & \dots & \dots & \dots \\ \theta_c^{m-1} \phi & \theta_c^{m-1} \phi^3 & \dots & \theta_c^{m-1} \phi^{2n-1} \end{pmatrix}. \tag{36}$$

In the discrete-time implementation of the online stiffness estimator, the unknown parameter vector $\hat{\boldsymbol{\eta}}$ will be identified using the algorithm (23), where $\hat{\boldsymbol{\alpha}}(k)$ is now replaced by $\hat{\boldsymbol{\eta}}(k)$. The stiffness estimate at time $t_k = kT$ is provided again by the relation (24), suitably modified according to Equation (35):

$$\begin{aligned} \hat{\sigma}(\theta_c(k), \phi(k)) &= \frac{\partial f(\theta_c(k), \phi(k))}{\partial \phi(k)} = \left(\frac{\partial \mathbf{F}(k)}{\partial \phi(k)} \right)^T \hat{\boldsymbol{\eta}}(k) \\ &= \sum_{i=0}^{n-1} \sum_{j=0}^{m-1} (2i+1) \hat{\eta}_{i,j}(k) \theta_c^j(k) \phi^{2i}(k). \end{aligned} \tag{37}$$

At this stage, it is immediate to realize that we can also remove de facto the restricting assumptions that we have preliminarily introduced, namely the separability condition (31) and the symmetric condition (32). The re-parametrization by $\boldsymbol{\eta}$ in (35) and a complete polynomial expansion in terms of $\theta_c^j \phi^i$ (with $j = 0, \dots, m-1$ and $i = 0, \dots, n-1$) to be used in place of (36) will cover the most general case. Nonetheless, we preferred introducing the above conditions, and the associated reduced expansion (36), since we observed that they were able to capture at best the flexibility behavior of the AwAS, our target serial VSA device, both in simulations and experiments.

5. Handling poor excitation conditions

For a robust parameter estimation, it is important that the range of processed signals is sufficiently large so that the collected data will contain enough information to fully explore the dynamic characteristics of the physical quantity to be estimated.⁸ When applied to an antagonistic VSA, the RLS algorithm is not very sensitive to poor excitation because the deformation of the two transmissions are significant in order to command/control simultaneously both link motion and stiffness. Instead, in a serial VSA the deformation can be minimal and the requirement of sufficient excitation is a very critical issue for stiffness estimation. Since the RLS estimation may become unstable in the presence of poor excitation, we have used in all cases the modified RLS scheme proposed by Bittanti et al. (1990). This is briefly recalled here with our notation for the readers' convenience.

Assume that the measured data y are generated at $t_k = kT$ in a deterministic way as

$$y(k) = \mathbf{F}^T(k) \bar{\boldsymbol{\alpha}}, \tag{38}$$

where $\bar{\boldsymbol{\alpha}}$ is the true but unknown parameter vector. In the parameter estimation error $\tilde{\boldsymbol{\alpha}} = \hat{\boldsymbol{\alpha}} - \bar{\boldsymbol{\alpha}}$, it is possible to discriminate a component $\tilde{\boldsymbol{\alpha}}_U$ that belongs to the so-called unexcitation subspace and a component $\tilde{\boldsymbol{\alpha}}_E$ that belongs to its orthogonal complement $\Omega_E = \Omega_U^\perp$, the excitation subspace. The following modification to the RLS algorithm (23) is used for the estimate $\hat{\boldsymbol{\alpha}}$:

$$\begin{aligned} \hat{\boldsymbol{\alpha}}(k) &= \hat{\boldsymbol{\alpha}}(k-1) + a(k) \mathbf{K}(k) \boldsymbol{\epsilon}(k), \\ \mathbf{P}(k) &= \mathbf{P}(k-1) - a(k) \mathbf{K}(k) \mathbf{F}^T(k) \mathbf{P}(k-1), \end{aligned} \tag{39}$$

where the scalar $a(k)$ is a time-varying function.

Under the data generation assumption (38), Bittanti et al. (1990) have proved that, if there exists a scalar $c > 0$ such that

$$\frac{a(k)}{1 + \rho(k) - a(k)\rho(k)} \geq c, \quad \forall k, \quad (40)$$

with $\rho(k)$ defined in (23), then, for every given $\hat{\alpha}(0)$ and $P(0) > 0$:

1. $\|\tilde{\alpha}(k)\| \leq \lambda$, $\forall k$, being λ a suitable positive constant;
2. $\lim_{k \rightarrow \infty} \tilde{\alpha}_E(k) = \mathbf{0}$.

Provided that $a(k)$ can be chosen so as to verify condition (40), we thus obtain practical convergence of the parameter estimation even in poor excitation cases. Given a constant $c > 0$, the stability factor $a(k)$ is then simply chosen as

$$a(k) = \frac{c + c\rho(k)}{1 + c\rho(k)}. \quad (41)$$

Summarizing, the enhanced RLS algorithm is obtained from (23), by replacing the last two equations therein with (39) and using (41).

6. Evaluation by simulation

In order to test the effectiveness of the estimator, we performed extensive simulations in discrete time for the VSA-II and the AwAS devices, using Matlab/Simulink. Actuators and sensors are modeled under realistic conditions, by considering encoder quantization, a noisy motor torque τ for the residual computation (17), as well as a noisy sensed flexibility torque $\tau_e(\phi)$, to be used in alternative to the residual as input $\hat{\tau}_e(\phi)$ for the RLS algorithm (23). We denote noisy signals with a tilde, i.e.

$$\tilde{\tau} = \tau + v_\tau, \quad (42)$$

$$\tilde{\tau}_e(\phi) = \tau_e(\phi) + v_{\tau_e}, \quad (43)$$

where v_τ and v_{τ_e} are zero mean Gaussian noises.

To illustrate the robustness of the method, we performed stiffness estimation in three modalities, using three different signals as input $\hat{\tau}_e(\phi)$ for the RLS algorithm. In the MODEL modality, we used as input the flexibility torque as obtained from the model of the flexible transmission and computed with the nominal system data. In the SENSOR modality, we used as input the flexibility torque measured by a noisy joint torque sensor, see Equation (43). Finally, in the RESIDUAL modality we fed the RLS algorithm with the residual that estimates the flexibility torque. In this last modality, the residual (17) has been evaluated using the noisy motor torque (42) and with motor position θ and velocity $\dot{\theta}$ obtained from quantized encoder data processed by the MKKF of Section 3.1. Summarizing, for the three modalities we have

$$\begin{aligned} \hat{\tau}_e(\phi) &= \tau_e(\phi) && \text{MODEL,} \\ \hat{\tau}_e(\phi) &= \tilde{\tau}_e(\phi) && \text{SENSOR,} \\ \hat{\tau}_e(\phi) &= r_e \text{ (including Equation (42))} && \text{RESIDUAL.} \end{aligned} \quad (44)$$

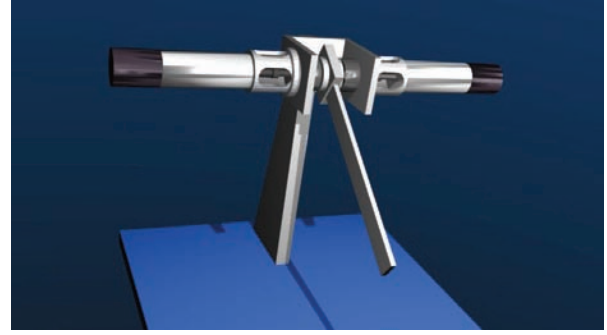


Fig. 3. CAD model of the antagonistic VSA-II driving a link under gravity.

To quantify stiffness estimation performance, we considered two indices, the mean square error (MSE) and the (dimensionless) mean square relative error percentage (MSREP) over p samples:

$$\text{MSE} = \frac{\sum_{k=0}^p [(\sigma(k) - \hat{\sigma}(k))^2]}{p}, \quad (45)$$

$$\text{MSREP} = \frac{\sum_{k=0}^p \left[\left(\frac{\sigma(k) - \hat{\sigma}(k)}{\sigma(k)} \right)^2 \right]}{p} \cdot 100. \quad (46)$$

6.1. Antagonistic case: VSA-II

The VSA-II device developed by the University of Pisa (Schiavi et al., 2008) consists of two motors in antagonistic arrangement, driving a link via two nonlinear transmissions arranged in a parallel configuration. The nonlinearity of each flexible transmission is obtained thanks to a pair of four-bar mechanisms with a linear spring.

The nonlinear flexibility torque of the two transmissions of the VSA-II is modeled as

$$\tau_{e,i}(\phi_i) = 2k_i \beta(\phi_i) \frac{\partial \beta(\phi_i)}{\partial \phi_i}, \quad i = 1, 2, \quad (47)$$

where k_i is the (constant) stiffness of the spring in the i th transmission, and

$$\beta(\phi_i) = \arcsin \left(C_i \sin \left(\frac{\phi_i}{2} \right) \right) - \frac{\phi_i}{2}, \quad i = 1, 2, \quad (48)$$

being $C_i > 1$ a geometric parameter of the four-bar mechanisms. Owing to the antagonistic arrangement, the total flexibility torque acting on the link dynamics is given by the sum in Equation (9).

The VSA-II dynamic model is given by Equations (7)–(8), with the parameter data presented by Schiavi et al. (2008). The driven link moves in the vertical plane, i.e. in the presence of gravity (Figure 3). We have considered encoders with $\Delta = 4,059$ pulses/turn for measuring q , θ_1 , and θ_2 .

The two motors are commanded by the sinusoidal torques $\tau_1(t) = 50 \cdot \sin 0.1\pi t$ and $\tau_2(t) = 50 \cdot \sin 2\pi t$ [Nmm], respectively. We have chosen a slow and a fast frequency to

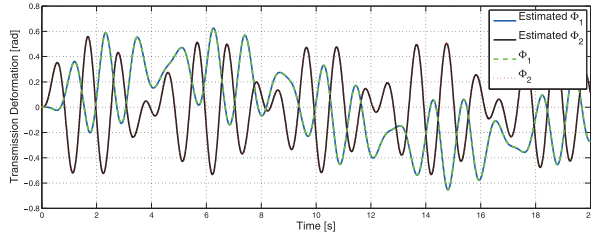


Fig. 4. Actual deformations ϕ_1 and ϕ_2 (dashed) of the two transmissions of the VSA-II and their estimation (solid, practically superposed) obtained using the MKKF on the measured position of the link and motors.

illustrate different excitation conditions for the two transmissions. The simulation runs with a sampling time $T = 1$ ms, starting from $q(0) = \theta_1(0) = \theta_2(0) = 0$ [rad] (lower equilibrium configuration) and with the system initially at rest.

The MKKF parameters in Equation (20) were chosen as $V_{\max} = 10$, $V_{\min} = 0.1$, and $\alpha = 6$, obtained by considering a nominal minimum and maximum velocity. The other estimation parameters were: $K_I = 300$ in Equation (17), which represents the filter bandwidth of the residual; $\mathbf{P}(0) = 10^6 \mathbf{I}_{n \times n}$ (large covariance) and $\boldsymbol{\alpha}(0) = \mathbf{0}$ (no a priori knowledge on actual parameters) for the initialization of the RLS algorithm in Equation (23); $n = 4$ in Equation (26), the order of the polynomial approximation (with odd powers only); and $c = 10^{-5}$ in Equation (41), for the enhanced RLS.

Figure 4 shows the actual time behavior of the two transmission deformations ϕ_1 and ϕ_2 under the applied motor torques τ_1 and τ_2 . The perfect reproduction obtained despite the noisy measurements used for the position of the link and motors shows the effectiveness of the MKKF algorithm. Note that even if the second motor is commanded by a torque having frequency 20 times larger than that on the first motor, the deformation of the two transmissions have a similar frequency behavior, due to the coupling.

Figure 5 compares the actual (nominal) evolution of the flexibility torques $\tau_e(\phi)$ of the VSA-II and their estimations obtained from noisy measure by joint torque sensor, using the residual, and processing the residual via the RLS algorithm. In particular, both the measured flexibility torque and its estimation obtained directly from the residual are quite noisy under the assumed operative conditions. However, a reliable (filtered and centered) flexibility torque estimation is obtained when feeding the residual into the RLS algorithm.

The time behavior of the stiffnesses estimated with the different modalities are reported in Figure 6, compared with their actual evolutions. The fast convergence rates and good steady tracking of the actual stiffness is obtained, despite the presence of encoder quantization and noisy measures. All methods provide a good stiffness estimation after a short transient phase, and in particular no tangible degradation is noticed when no joint torque sensor is used. This result is

confirmed by the similar performance indices reported in Table 1.

Figure 7 shows the behavior of the $n = 4$ coefficients of vector $\hat{\boldsymbol{\alpha}}$ that characterize the polynomial $f(\phi, \hat{\boldsymbol{\alpha}})$. After an initial transient phase, all coefficients reach a constant regime. The last coefficient $\hat{\alpha}_3$ (weighting the term ϕ^7) remains practically negligible. Finally, the characteristic curves of the final estimated model $f(\phi, \hat{\boldsymbol{\alpha}})$ for the flexibility torques of the two transmissions obtained are plotted in Figure 8 against the sampled data points (represented with crosses) collected during simulation, i.e. the flexibility torques estimated using the residual.

6.2. Serial case: AwAS

The AwAS serial device adjusts the stiffness at the joint through the variation of the relative distance between a pair of springs and the center of rotation of the joint, using a lever mechanism. A CAD model with a description of the components is shown in Figure 9.

The dynamic model of the AwAS is described by Equations (12), where the flexibility torque $\tau_e(r, \phi)$ and the stiffness $\sigma(r, \phi)$ are defined by

$$\tau_e(r, \phi) = k_s r^2 \sin 2\phi \tag{49}$$

and

$$\sigma(r, \phi) = 2k_s r^2 \cos 2\phi, \tag{50}$$

where k_s is the stiffness of the springs and r is the length of the lever arm, which is the actual distance between the center of rotation of the joint and the springs. The lever arm is adjusted by the secondary motor as

$$r = r_0 - b\theta_c, \tag{51}$$

where r_0 is the initial length of the lever arm, θ_c is the angular position of the motor, and b is the transmission ratio between the secondary motor and the ball screw. Finally, the torque that the transmission applies back to the secondary motor is given by

$$\psi_e(r, \phi) = -2k_s b r \sin^2 \phi. \tag{52}$$

We note that the length r of the lever arm in Equation (51) can be directly used in place of θ_c in all of the expressions of Section 4, and in particular in the RLS estimation algorithm. With reference to Equations (12) and (49)–(52), and with the link moving on the horizontal plane ($g(q) \equiv 0$), the nominal parameters of the AwAS are

$$\begin{aligned} M &= 0.1, B_m = 2.3 \cdot 10^{-5}, B_{m,c} = 1.29 \cdot 10^{-7} \text{ [kg} \cdot \text{m}^2\text{]}, \\ D_q &= 0.15, D_{\theta,m} = 0.001, D_{\theta,m,c} = 0.0141 \text{ [N} \cdot \text{m} \cdot \text{s/rad]}, \\ \gamma &= 50, \gamma_c = 23, k_s = 0.01422 \text{ [kN/mm]}, \\ r_0 &= 100 \text{ [mm]}, b = 2.5/2\pi \text{ [mm/rad]}. \end{aligned} \tag{53}$$

We have considered encoders with $\Delta = 40,000$ pulses/turn for measuring q and θ , and with $\Delta_c = 1,024$ for θ_c . The simulation runs with a sampling time $T = 1$ ms, starting at rest from $q(0) = \theta(0) = \theta_c(0) = 0$ [rad] and using as torque inputs $\tau_m = 0.3 \cdot \sin 0.2\pi t$ [Nm] for the primary motor and the torque profile shown in Figure 10 for the secondary motor.

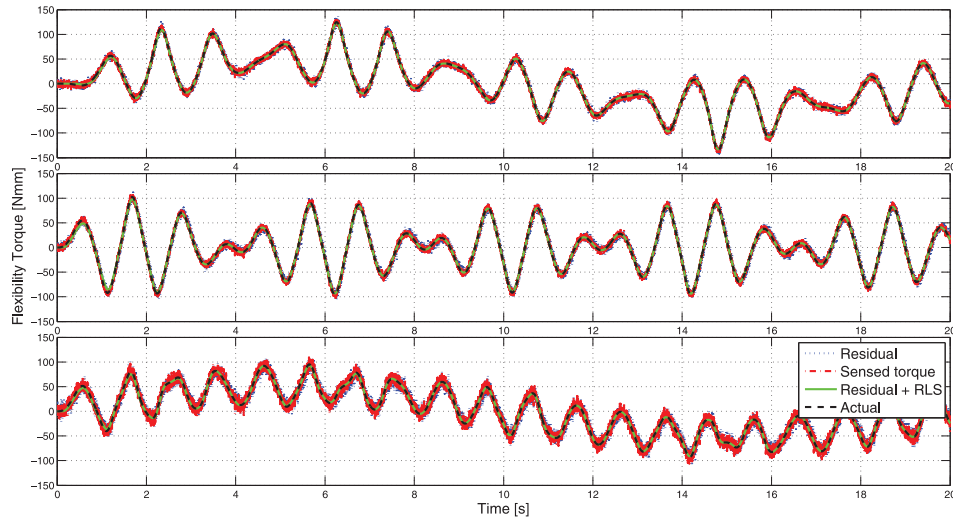


Fig. 5. Comparison of the flexibility torque for the first transmission (top), second transmission (middle), and total VSA-II device (bottom): actual $\tau_e(\phi)$ (dashed, black), estimated from the residual r_e (dotted, blue), measured by a noisy torque sensor $\tilde{\tau}_e(\phi)$ (dashed, red), and obtained from the RLS algorithm as $f(\phi, \hat{\alpha})$ using the residual as input (solid, green).

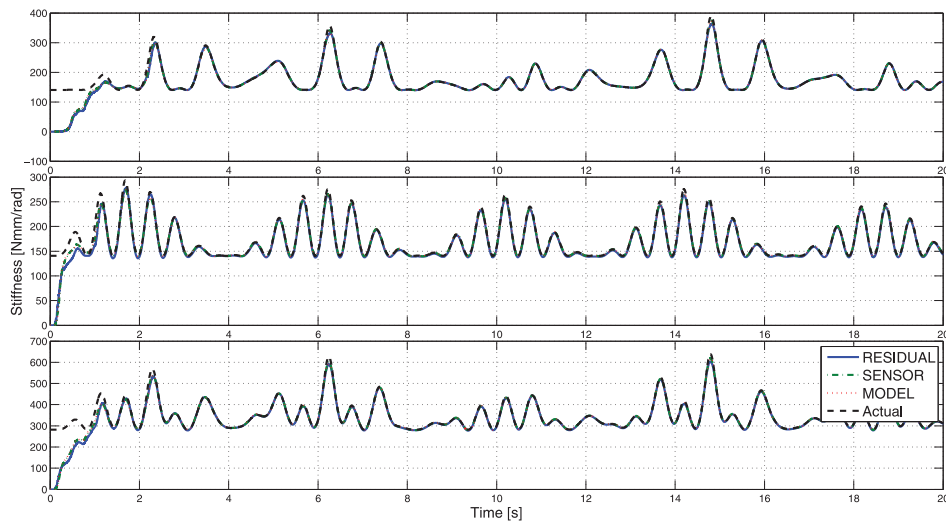


Fig. 6. Comparison of the stiffness for the first transmission (top), second transmission (middle), and total VSA-II device (bottom): actual σ (dashed, black), MODEL estimation (dotted, red), SENSOR estimation (dot-dashed, green), and RESIDUAL estimation (solid, blue).

Table 1. Performance of the total stiffness estimation for the VSA-II using three different modalities.

	MODEL			SENSOR			RESIDUAL		
	1	2	Total	1	2	Total	1	2	Total
MSE [Nmm ² /rad ²]	20.1	11.1	50.1	21.8	12.4	55.2	37.4	25.2	92.2
MSREP [%]	0.05	0.02	0.026	0.049	0.02	0.027	0.07	0.05	0.046

The MKKF parameters in Equation (20) and the residual gain in Equation (17) were the same as in the VSA-II case. The RLS algorithm in Equation (23) has been initialized with $P(0) = 10^{20}I_{(n-m) \times (n-m)}$ and $\hat{\eta}(0) = \mathbf{0}$, while $c = 10^{-20}$ has been used in Equation (41) for enhancing the

RLS scheme. The number of model parameters in Equation (33) was set to $n = 6$ and $m = 3$, so that the parameter vector η has dimension $n \cdot m = 18$. The orders m and n of the polynomial approximations have been selected on the basis of the nominal model (49).

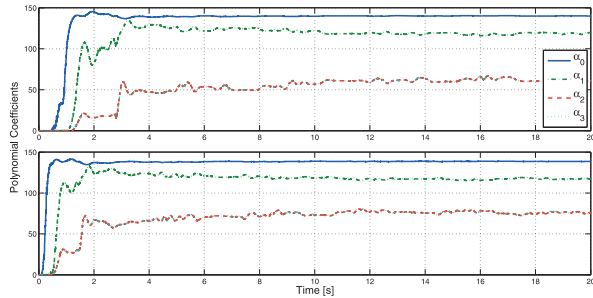


Fig. 7. Evolution of the polynomial model coefficients during estimation for the first (top) and second (bottom) transmission of the VSA-II.

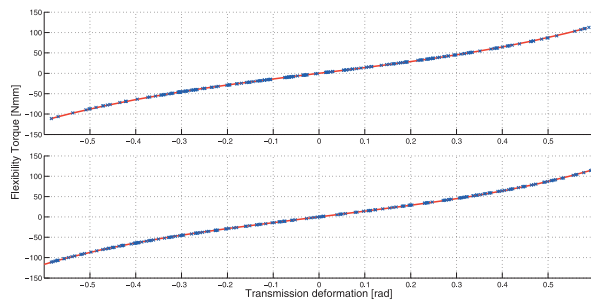


Fig. 8. Characteristic curve of the flexibility torque as a function of the deformation for the first (top) and second (bottom) transmission of the VSA-II: profile obtained with the final estimated polynomial model (solid, red) and collected data during simulation (crosses, blue).

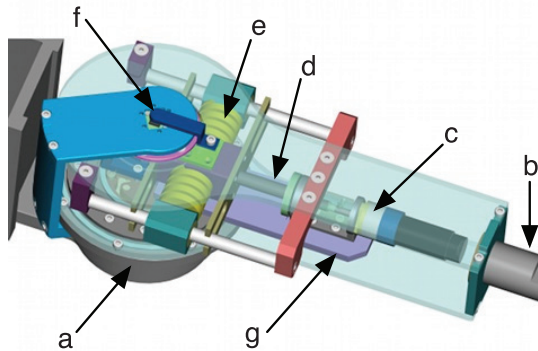


Fig. 9. CAD model of AwAS. The primary motor (a) rotates the intermediate link (g) around the joint axis of rotation (f); the secondary motor (c) drives a ball screw mechanism (d), which moves the relative position of a pair of antagonistic springs (e) with respect to the center of rotation of the joint (f); the springs connect both the output link (b) and the intermediate link (g).

Figure 11 shows the time behavior of the transmission deformation ϕ during the simulation. Note that its maximum value is very small (of the order 0.005 rad) and we are thus in a situation of very poor excitation for the RLS algorithm. Furthermore, the benefit of MKKF processing

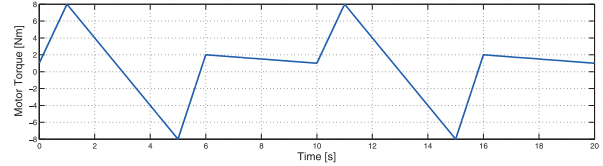


Fig. 10. Commanded torque $\tau_{m,c}$ for the secondary motor of the AwAS.

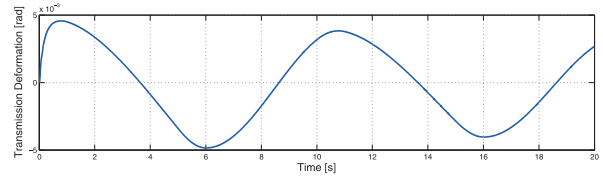


Fig. 11. Transmission deformation ϕ of the AwAS.

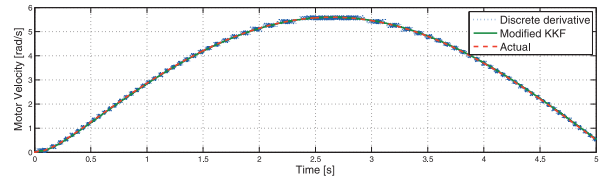


Fig. 12. Motor angular velocity $\dot{\theta}$ of the AwAS: actual (dashed, red), obtained with numerical differentiation (dotted, blue), and estimated with MKKF (solid, green).

of the encoder data can be appreciated from Figure 12. The primary motor velocity $\dot{\theta}$ obtained by numerical differentiation of the encoder position data suffers from the presence of quantization.

Figure 13 compares the actual evolution of the flexibility torque $\tau_e(r, \phi)$ of the AwAS with two different estimation modalities and the measure from the joint torque sensor. As in the VSA-II case, the measured and the estimated flexibility torque obtained directly from the residual (17) are quite noisy. The best result is obtained when feeding the residual into the RLS algorithm and using the estimated parameter vector $\hat{\eta}$ in Equation (35).

The time behavior of the stiffness estimated with the different modalities is reported in Figure 14, compared with its actual evolution. From the performance results in Table 2, all methods perform similarly well. With these simulation results, the MODEL stiffness estimate is indeed very accurate despite the presence of encoder quantization. The SENSOR estimation is also very accurate, confirming the benefit of using anyway a sensor data processing by the enhanced RLS algorithm. The RESIDUAL estimation has a higher MSE, due to the propagation of input noise through the two stages of the estimation process; however, its MSREP is still less than 0.1% which allows to conclude that torque sensing is not strictly needed.

Figure 15 shows the behavior of the most relevant coefficients $\hat{\eta}_{i,j}$ that characterize the polynomial $f(r, \phi, \hat{\eta})$. After a fast transient phase, all coefficients become practically constant. Furthermore, the single dominant coefficient $\hat{\eta}_{0,2}$

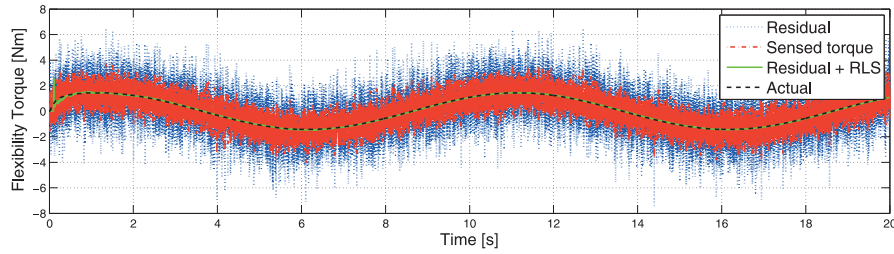


Fig. 13. Comparison of the flexibility torque of the AwAS transmission: actual $\tau_e(r, \phi)$ (dashed, black), estimated from the residual r_e (dotted, blue), measured by a noisy torque sensor $\tilde{\tau}_e(r, \phi)$ (dot-dashed, red), and obtained from the RLS algorithm as $f(r, \phi, \hat{\eta})$ using the residual in input (solid, green).

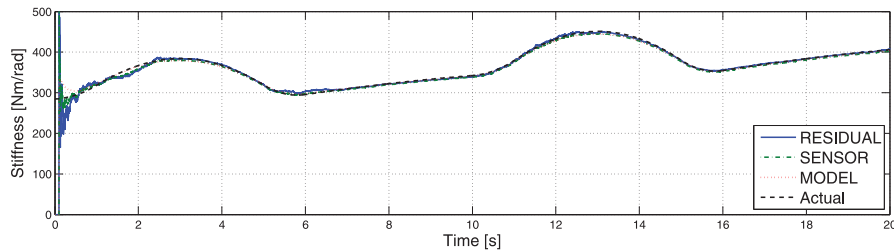


Fig. 14. Comparison of the device stiffness $\sigma(r, \phi)$ of the AwAS: actual (dashed, black), MODEL estimation (dotted, red), SENSOR estimation (dot-dashed, green), and RESIDUAL estimation (solid, blue).

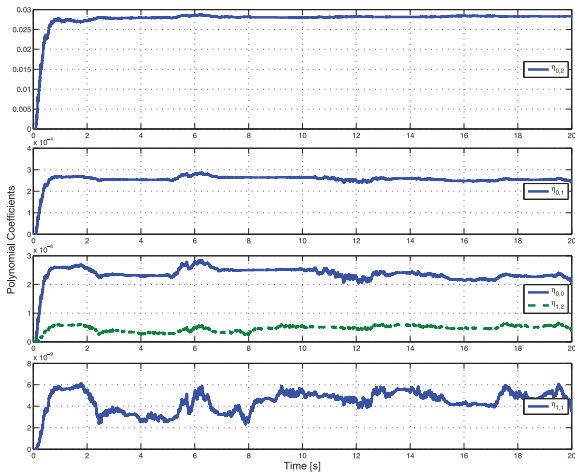


Fig. 15. Evolution of the polynomial model coefficients $\hat{\eta}_{i,j}$ during estimation for the AwAS.

Table 2. Performance of the AwAS stiffness estimation using three different modalities.

Estimation	MSE [Nm ² /rad ²]	MSREP [%]
MODEL	7.84	0.005
SENSOR	14.92	0.01
RESIDUAL	18.97	0.05

stabilizes around the value 0.0284, whereas all other coefficients can be neglected (note the different scales). Therefore, the approximating polynomial model (35) can be reduced to $f(r, \phi, \hat{\eta}) \simeq \hat{\eta}_{0,2} \phi r^2$. Considering a situation of small transmission deformations in the nominal model (49)

of the flexibility torque of the AwAS we obtain $\tau_e(r, \phi) \simeq 2k_s \phi r^2$. It is not surprising that in fact $2k_s = 0.0284 = \hat{\eta}_{0,2}$ (expressed in [kN/mm]), namely that the estimator has accurately identified the dominant characteristic of the flexible transmission. Finally, the characteristic surface of the flexibility torque is shown in Figure 16 as a function of the transmission deformation and the lever arm. This surface represents the final estimated model $f(r, \phi, \hat{\eta})$, while the crosses are the data points of the actual flexibility torque sampled during the simulation.

6.3. Multi-DOF case

Since the design of the stiffness estimation algorithm is performed on the motor side of the VSA, its decentralized extension to VSA-based robot with multiple degrees of freedom is straightforward. We briefly illustrate the performance of the same method used for single-DOF VSAs on a simple but representative example modeled by the dynamic equations (14). We consider a 2R manipulator moving in the vertical plane (with gravity), with both joints actuated by VSA-II devices having the same numerical parameters as in Section 6.1. The only extra parameter needed, namely the actuator mass $m_m = 0.345$ [kg] of the VSA-II at the second joint, is taken again from Schiavi et al. (2008). The robot links are modeled as two equal uniform thin rods with mass $m_l = 0.1$ [kg] and length $l = 0.5$ [m].

The first actuator is commanded by sinusoidal torques of common amplitude 50 [Nmm] and frequency 0.1 [Hz] for $\tau_{1,1}(t)$ and 0.2 [Hz] for $\tau_{1,2}(t)$. The second actuator is commanded by a sawtooth wave torque $\tau_{2,1}(t)$ with amplitude 50 [Nmm] and frequency 0.1 [Hz] and a square wave torque

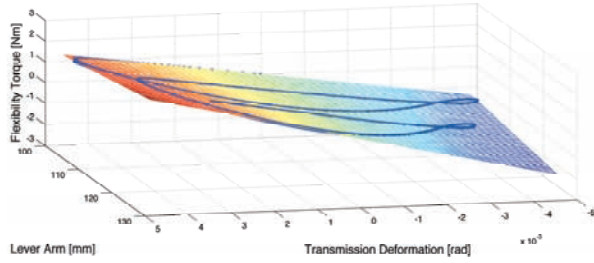


Fig. 16. Characteristic surface of the flexibility torque as a function of the transmission deformation ϕ and the lever arm r of the AwAS: 3D profile obtained with the final estimated polynomial model, with superposed data collected during the simulation (crosses, blue).

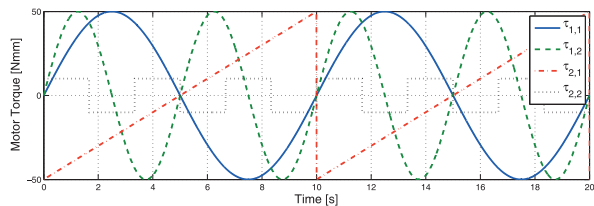


Fig. 17. Motor torques applied to the VSA-based 2R manipulator.

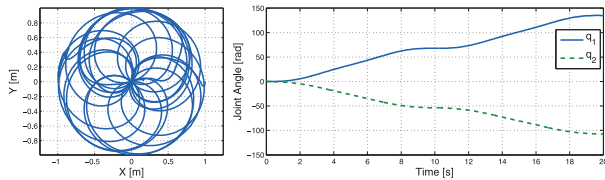


Fig. 18. End-effector path (left) and evolution of link angles q (right) associated with Figure 17.

$\tau_{2,2}(t)$ with amplitude 10 [Nmm] and frequency 0.3 [Hz]. Figure 17 shows the time profiles of the four motor torques. The resulting evolution of the link variables and the corresponding path executed by the end-effector (i.e. of the tip of the second link) are shown in Figure 18, which indicates that the whole robot workspace is being dynamically explored.

The estimator parameters used in the simulation are the same as in the single VSA-II case presented in Section 6.1. Figure 19 shows the estimated flexibility torques of the four transmissions (two at the first robot joint and two at the second joint), while the associated transmission stiffnesses are shown in Figure 20. Each behavior is very similar to the single-DOF case, confirming the independence of the proposed stiffness estimation method from the dynamic torques acting on the link sides of the transmissions.

7. Choice of parameters and robustness

We describe the role of the various parameters for the stiffness estimator following the order in which they were introduced in the paper, and provide some guidelines for their selection.

The residual estimator in Section 3.1 is characterized by the single parameter K_I , which is the -3 dB bandwidth of the low-pass filtered reconstruction of the flexibility torque. In fact, when rewriting Equation (16) in the Laplace domain we obtain the unitary first-order filter

$$\frac{r_e(s)}{\tau_e(s)} = \frac{1}{1 + \frac{1}{K_I}s} \tag{54}$$

with time constant $1/K_I$ equal to the inverse of the filter bandwidth. If the value K_I is too small, the filtering action will be too large and the signal may not be properly reconstructed. On the other hand, if it is too large then external noises may be amplified. In all performed simulations and experiments, the value $K_I = 300$ resulted in a reasonable compromise.

The MKKF in Equations (18)–(20) of Section 3.1 is characterized by four parameters: α , V_a , V_{\max} , and V_{\min} . The shape factor α changes the slope of the curve which represents the variance of the input noise. A good filtered response has been obtained with values of α ranging between 4 and 6. The kinematic filter is not particularly sensitive to the variance V_a . However, this value should be chosen so that the covariance matrix \mathbf{Q} of the filter state does not have too small values. In the simulations, we have chosen $V_a = 10^{10}$. The parameters V_{\max} and V_{\min} are related instead to the encoder resolution and to the range of velocities experienced by the motor. For a good estimation of the velocity, these values need to be tuned with respect to the actual encoder resolution. In the AwAS simulations, we considered the availability of an encoder with a good resolution (40,000 pulses/turn), and for this reason we have chosen $V_{\max} = 10$ and $V_{\min} = 0.1$. To simplify the choice of these two parameters, we may work assuming the presence of low-resolution encoders, thus having a large output noise variance R . This affects the convergence rate of the motor velocity estimation, but the stiffness estimator will still remain rather insensitive, thanks to the presence of filtering actions in the residual and in the RLS algorithm. In the robustness study presented further below, we will use the larger values $V_{\max} = 10^5$ and $V_{\min} = 10^4$.

The RLS algorithm in Section 3.2 depends on the initialization parameters $\hat{\boldsymbol{\alpha}}(0)$ (or $\hat{\boldsymbol{\eta}}(0)$) for serial VSAs such as the AwAS and $\mathbf{P}(0)$ (usually chosen as a positive scalar $p(0)$ times the identity matrix, i.e. $\mathbf{P}(0) = p(0)\mathbf{I}$), as well as on the scalar parameter $c > 0$ introduced in Equation (40) for the enhanced RLS version. During the tests, we have always assumed no a priori knowledge of the actual range or values of transmission stiffness, and we have set $\hat{\boldsymbol{\alpha}}(0) = \mathbf{0}$ or $\hat{\boldsymbol{\eta}}(0) = \mathbf{0}$ accordingly. The initialization of $\mathbf{P}(0)$ and the value of c are strongly correlated, and they both act on the convergence rate of the estimator. With a large $\mathbf{P}(0)$, the RLS will be more reactive and converge faster, but this fast reaction can produce an unstable behavior in conditions of poor excitation. On the other hand, choosing c close to zero prevents unstable behaviors in the enhanced RLS algorithm,

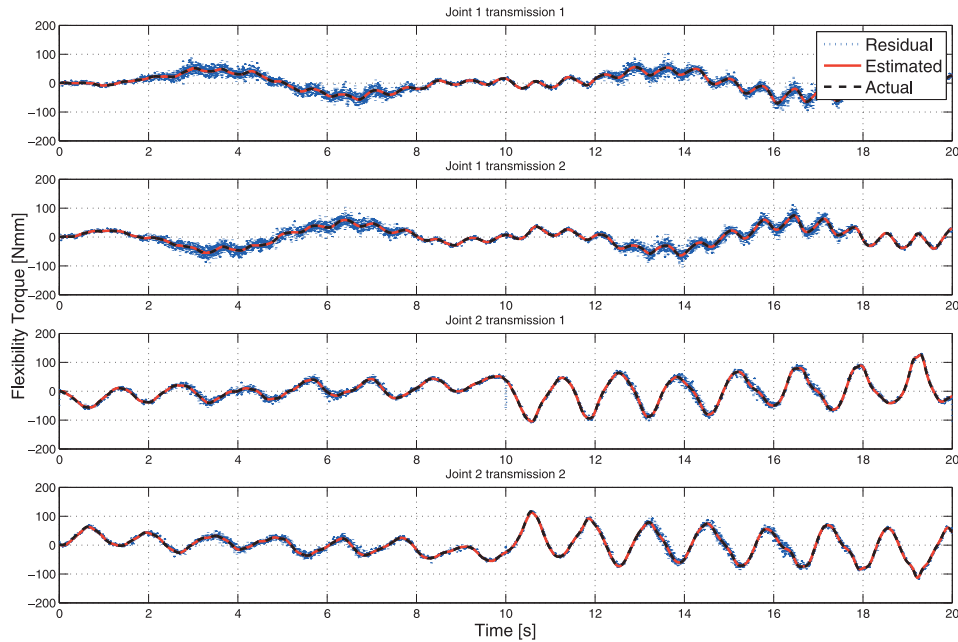


Fig. 19. Comparison of the four flexibility torques for the two VSA-II devices driving the 2R robot: actual $\tau_{e,1}(\phi_1)$ and $\tau_{e,2}(\phi_2)$ (dashed, black), estimated from the four-dimensional vector residual r_e (dotted, blue), measured by noisy torque sensors $\tilde{\tau}_{e,1}(\phi_1)$ and $\tilde{\tau}_{e,2}(\phi_2)$ (dashed, red), and obtained from the RLS algorithm as the vector function $f(\phi, \hat{\alpha})$ using the residuals as input (solid, green).

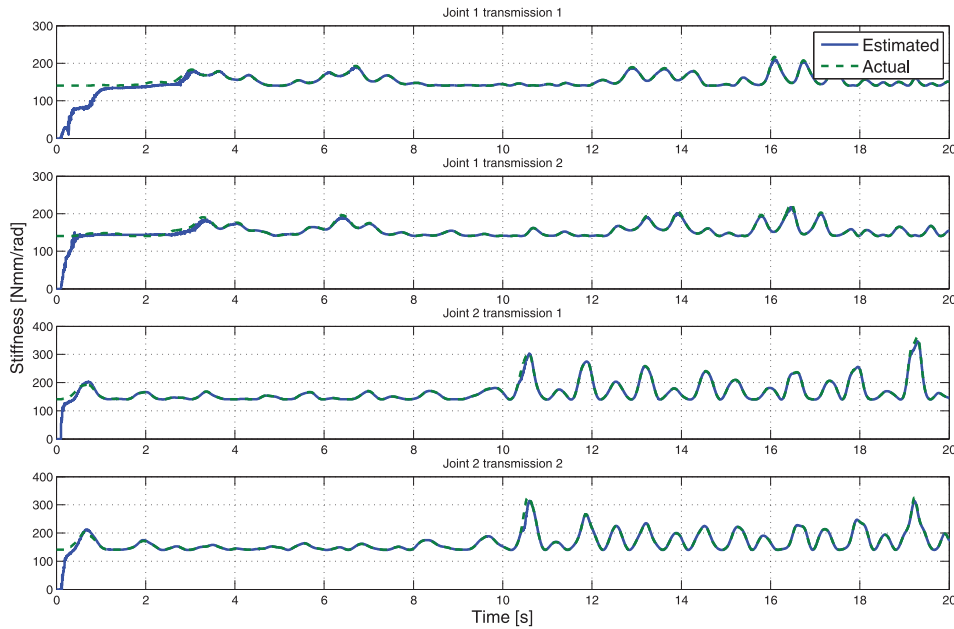


Fig. 20. Comparison of the four transmission stiffnesses σ for the two VSA-II devices driving the 2R robot: actual (dashed, green) and RESIDUAL estimation (solid, blue).

but the convergence is significantly slowed down. We found that the ratio between $p(0)$ and c^{-1} mostly affects the estimation convergence, and a good compromise is obtained when $p(0)c = 1$. This relation can be used to obtain initial values for these two parameters: it is then possible to

increase $P(0)$ when the system is sufficiently excited (typically, in the antagonistic case as for the VSA-II) in order to have faster convergence, or decrease c so as to improve the robustness of the estimator in the case of a poorly excited system.

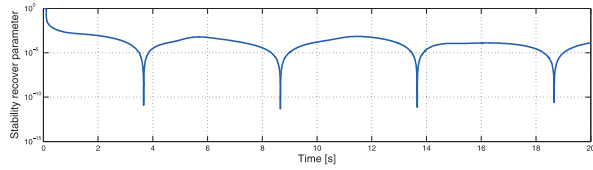


Fig. 21. Stability factor $a(k)$ in the RESIDUAL method for stiffness estimation on the AwAS (semi-logarithmic scale).

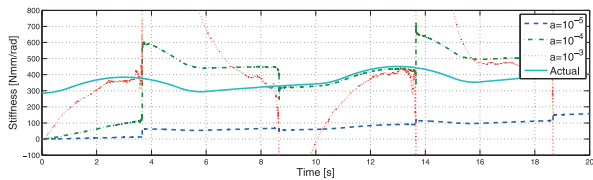


Fig. 22. AwAS stiffness estimated by RESIDUAL method and RLS for different constant factors a and for a time-varying $a(k)$ as in Equation (41).

To conclude the analysis of the parameters affecting convergence and robustness of the stiffness estimator, we evaluate the effects of the stability factor $a(k)$ introduced in Section 5 and the sensitivity of the method to the quality of position measurements. The relevance of a time-varying stability factor $a(k)$ for robustness is best assessed by considering the case of stiffness estimation for the AwAS in Section 6.2 as obtained using the RESIDUAL method. The time evolution of the stability factor during the online stiffness estimation is shown in Figure 21 on a semi-logarithmic scale. By comparing this with Figure 11, it is possible to note that the low peaks of $a(k)$ are associated with values of the transmission deformation that are close to zero. In such conditions, the Jacobian vector F^T will contain very small values, which implies a poor excitation for the estimator. As a matter of fact, the sudden reduction of $a(k)$ will compensate this adverse condition avoiding divergence of the estimator. This could not be achieved when using instead a constant factor $a(k) = a$, for all k . When the factor a is chosen small, the stiffness estimation is not affected by poor excitation but the convergence is very slow. On the other hand, with a constant and large a the convergence is faster but the estimation is very sensitive to poor excitation conditions. These behaviors are illustrated in Figure 22 for a range of constant values of a , justifying the relevance of using the enhanced RLS algorithm (39) with the time-varying stability factor $a(k)$ given by Equation (41).

To quantify the effects of the quality of encoder measurements on the proposed estimator, we have simulated both considered VSA systems with different encoder resolutions and verified the performance with the MSREP index (46). Having also assumed the presence of low-resolution encoders (in the range 10^2 – 10^4 pulses/turn), the variance of the input noise of the MKKF is high and thus we have used the larger parameters $V_{\max} = 10^5$ and $V_{\min} = 10^4$. From Figure 23 (for the VSA-II) and Figure 24

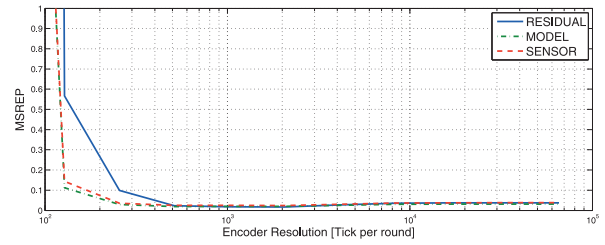


Fig. 23. MSREP obtained for the stiffness estimation of the VSA-II with different encoder quantization: MODEL estimation (dot-dashed, green), SENSOR estimation (dashed, red), and RESIDUAL estimation (solid, blue).

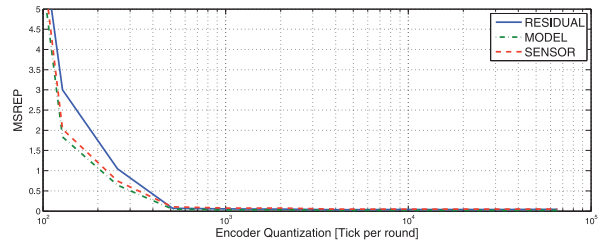


Fig. 24. MSREP obtained for the stiffness estimation of the AwAS with different encoder quantization: MODEL estimation (dot-dashed, green), SENSOR estimation (dashed, red), and RESIDUAL estimation (solid, blue).

(for the AwAS), it follows clearly that the RESIDUAL estimation has a greater MSREP in comparison with the SENSOR and MODEL estimations, especially at low encoder resolutions. This is due to the fact that the RESIDUAL estimator uses the encoder signal twice, in the residual computation itself and in the RLS algorithm. Note also that all estimators provide a good stiffness estimation for both VSA typologies already at a resolution of 1,024 pulses/turn. It is then possible to use an encoder with resolution as low as 256 pulses/turn, using quadrature detection. Finally, when comparing the results between the two VSA devices, the stiffness estimator for the serial AwAS has a higher MSREP due to a larger sensitivity to poor excitation conditions.

8. Experimental results

The stiffness estimation method has been tested through experiments using AwAS, see Figure 25, developed at the Istituto Italiano di Tecnologia (IIT) and presented by Jafari et al. (2010). The relative simplicity of the potential function associated with the transmission deformation of the AwAS and the presence of a sensor that measures the flexibility torque of the transmission, allowing an alternative validation of the results, makes this actuator a useful benchmark for evaluating our stiffness estimator.

In the experiments performed on a horizontal plane, the primary and secondary motors drive the AwAS with sinusoidal torque signals. The sampling time was $T = 1$ ms. The obtained lever arm position r and transmission deformation ϕ are shown in Figures 26 and 27, respectively.



Fig. 25. The AwAS used for the experimental tests.

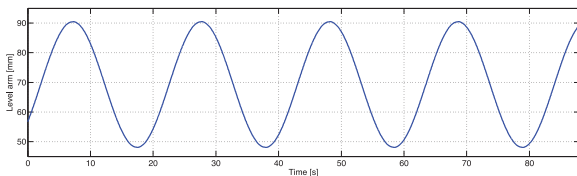


Fig. 26. Lever arm length r in the AwAS experiment.

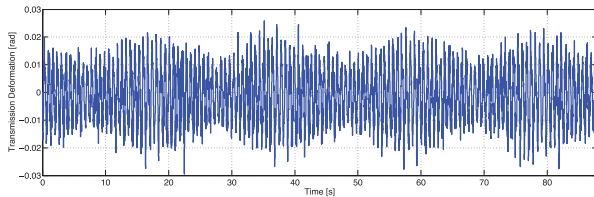


Fig. 27. Transmission deformation ϕ in the AwAS experiment.

To validate our estimation algorithm, we take advantage of the calibrated torque sensor available in the AwAS and we consider the flexibility torque measured by the torque sensor as the ground truth. The actual difference between the nominal flexibility torque, obtained from the model (49) with the data (53), and its measurement with the torque sensor is shown in Figure 28.

Figure 29 shows the stiffness estimation results, obtained with a parametric polynomial model for the flexibility torque in the form (35), with the length r of the lever arm in place of the secondary motor position θ_c , and using a vector $\hat{\eta}$ of $n \cdot m = 18$ coefficients. As in the simulations of Section 6, we have considered three different experimental estimation modalities (MODEL, SENSOR, and RESIDUAL) and compared them with the nominal stiffness expression given by Equation (50). We remark that in this case the MODEL estimation uses the nominal expression (49) of the flexibility torque evaluated with the measured transmission deformation ϕ for feeding the RLS algorithm, providing thus some filtering action. In the SENSOR and RESIDUAL modalities, the RLS works with the measured flexibility torque and with the reconstructed one from the residual computation (17), respectively.

It is worth noting that the nominal flexibility torque, obtained using Equation (49) and the nominal AwAS data given in Section 6.2, differs from the real flexibility torque of the AwAS due to unmodeled dynamics and uncertain knowledge of the model parameters. This will also be reflected in a difference between the real stiffness and the nominal one. Indeed, the MODEL estimation method is very accurate in tracking the nominal stiffness (the two traces are practically superposed in Figure 29) and the comparison of these two obtained results provides $MSE = 9.36$ and $MSREP = 0.034\%$ as performance indices. Stated differently, if the nominal stiffness was the real one, the MODEL estimation method would work properly.

On the other hand, the results from the SENSOR estimation method, that we assume to provide the real ground truth for the AwAS stiffness, show a sensible difference with respect to the nominal stiffness and therefore the actual need for an independent stiffness estimator. The stiffness estimation by the RESIDUAL method is quite accurate in reproducing the SENSOR estimation results. Their relative comparison in terms of performance indices yields $MSE = 63.02$ and $MSREP = 1.55\%$. However, we have to consider that SENSOR and RESIDUAL estimation modalities are the result of the RLS, which has the same convergence behavior for both estimations.

Figure 30 shows the time behavior of the most relevant coefficients $\hat{\eta}_{i,j}$ that characterize the polynomial $f(r, \phi, \hat{\eta})$, namely the estimates of $\eta_{0,0}$ (weighting ϕ), $\eta_{0,1}$ (weighting ϕr), $\eta_{0,2}$ (ϕr^2), $\eta_{1,1}$ ($\phi^3 r$), and $\eta_{1,2}$ ($\phi^3 r^2$). The single dominant coefficient $\hat{\eta}_{0,2}$, after an initial jerky transient phase, becomes practically constant (representing the main contribution to $2k_s$ in Equation (50)). From this value, we can also estimate the main parameter in the AwAS transmission, the spring stiffness, as $k_s = 0.0107$ [kN/mm]. Removing the contribution due to the dominant $\hat{\eta}_{0,2}$, all remaining coefficients $\hat{\eta}_{i,j}$ collectively result in a torque of the order of 10^{-17} Nm, as shown in Figure 31, and are thus completely negligible.

The characteristic surface of the flexibility torque expressed as a function of the transmission deformation and the lever arm is shown in the top part of Figure 32. This surface represents the final estimated model $f(r, \phi, \hat{\eta})$ at the end of the experiment, while the crosses are the data points of the actual flexibility torque sampled during the experiment. The second, third, and fourth plots represent slices of the flexibility torque characteristic at fixed lever arm length, respectively with r equal to 50, 70, and 90 [mm], superposed with the associated data collected during the experiment. From the varying slope of these plots one can clearly recognize the decoupled property of the serial AwAS, with the auxiliary variable r commanded by the secondary motor varying the stiffness of the device, independently from the link motion (and associated transmission deformation) imposed by the primary motor.

In order to provide a final validation of the obtained stiffness estimation results, we need to perform an independent

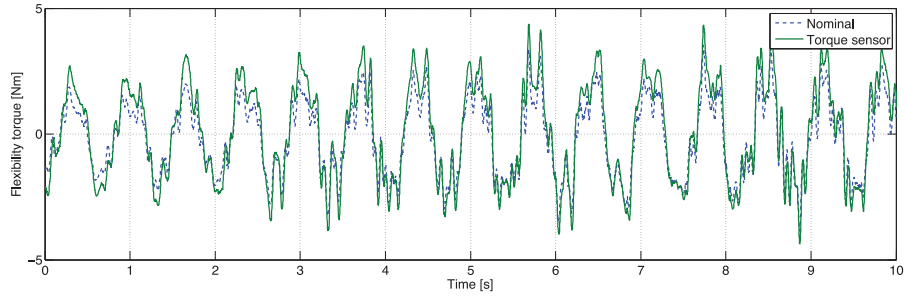


Fig. 28. Flexibility torque in the AwAS experiment: nominal (dashed, blue) and measured by the torque sensor (solid, green); expanded view for 10 s.

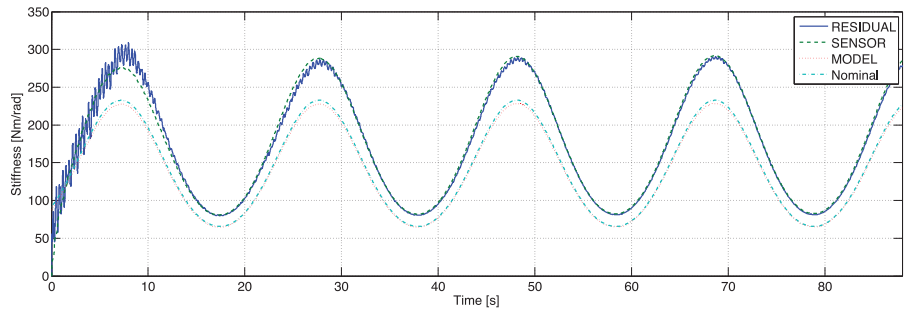


Fig. 29. Estimated stiffness in the AwAS experiment: nominal (dot-dashed, green), MODEL estimation (dotted, red), SENSOR estimation (dashed, green), and RESIDUAL estimation (solid, blue).

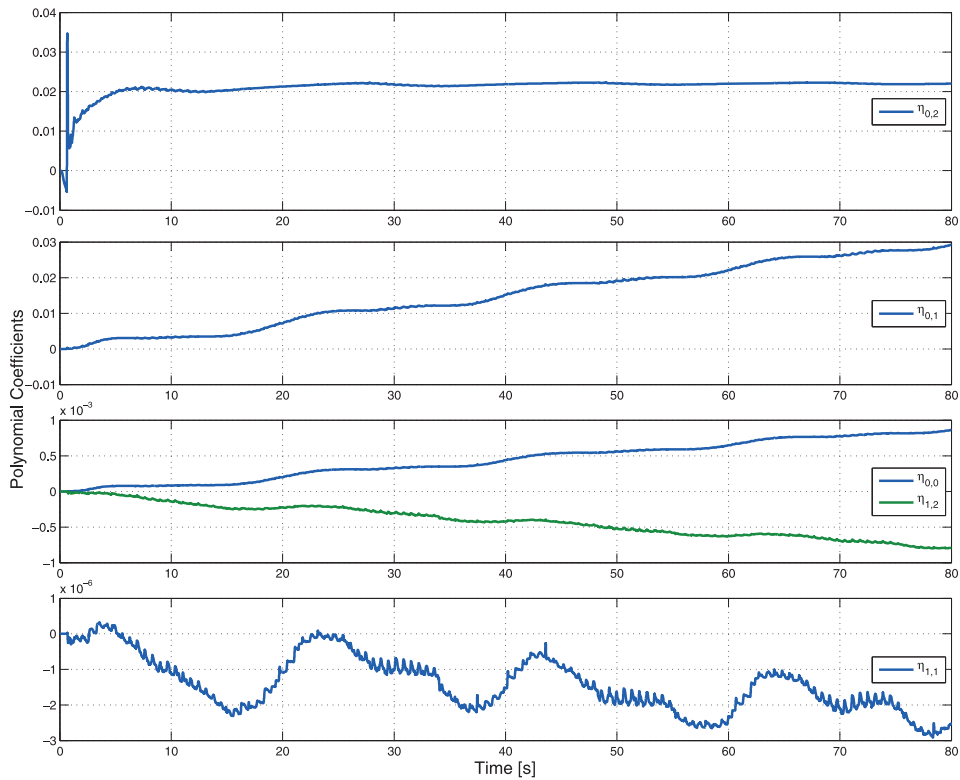


Fig. 30. Evolution of the first five most relevant coefficients $\hat{\eta}_{i,j}$ in the polynomial model of the flexibility torque for the AwAS experiment.

experiment with different input motor torques and compare the collected data against the parametric model of the

stiffness estimated in the previous experimental test. From the performed analysis and the results obtained so far, this

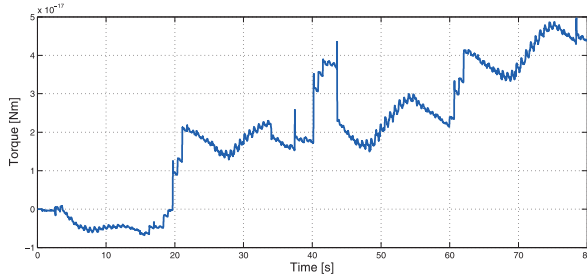


Fig. 31. Torque contribution to the flexibility torque estimate provided collectively by all considered coefficients $\hat{\eta}_{i,j}$, except for the dominant $\hat{\eta}_{0,2}$.

comparison can be reliably made on the flexibility torque, between that measured by the joint torque sensor available on the AwAS during the new experiment and the previous estimated expression of its parametric model, evaluated with the new transmission deformations and lever arm positions. This procedure satisfies two validation principles that are relevant in the considered framework: the separation between the data sets used for estimation and for validation; and the dynamic nature of the tests associated with the actual time-varying operative conditions of the VSA device (as opposed to a quasi-static validation of the estimated stiffness).

Based on these considerations, we have conducted a new experiment using as inputs to the system a different torque produced by the primary motor of the AwAS and a sinusoidal torque similar to the previous experiment delivered by the secondary motor. The resulting lever arm length and transmission deformation are shown in Figure 33 and 34, respectively. Comparing the latter with Figure 27, we note that the time profile of the deformation ϕ has changed and its peaks are now doubled in amplitude.

Figure 35 shows the time behavior of the flexibility torque as computed by the previously estimated parametric model and as measured in the second experiment by the joint torque sensor. Indeed, the parametric model is not updated during this experiment. Finally, the characteristic surface of the AwAS flexibility torque obtained using the polynomial model estimated in the previous experiment is reported in Figure 36 as a function of the transmission deformation ϕ and the lever arm r . The data points of the flexibility torque measured with the torque sensor during the validation experiment are represented with crosses, showing a good match with the estimated characteristic surface. Therefore, also the stiffness estimation obtained via analytical differentiation of the parametric model, as in Equation (4), is expected to be reliable. We stress that these satisfactory results were obtained despite our stiffness estimation method is mainly intended for an online use, i.e. for capturing on the fly any new variation of the stiffness characteristics.

9. Conclusions

We have presented a unified approach to the online estimation of the time-varying stiffness in VSA devices driven by two electrical motors and nonlinear flexible transmissions arranged in typical antagonistic or serial configurations. The proposed method does not require the introduction of joint torque sensors nor the numerical differentiation of measurements (in particular, to obtain acceleration), as opposed to other existing stiffness estimation techniques.

The estimation procedure is organized in two stages. First the flexibility torque is reconstructed through a residual signal on the basis of motor parameters (inertia, damping), commanded signal (torque/current), and link and motor position measurements, with motor velocity obtained through a MKKF. The residual provides a first-order low-pass filtered estimate of the flexibility torque of the transmission.

Stiffness estimation is then completed in the second stage using a RLS algorithm based on a linearly parametrized model, with polynomial dependence on the deformations (and on the position of the auxiliary motor for VSA in serial configuration). The RLS algorithm can take as input the flexibility torque estimated by the residual in the first stage, or the measured torque when a joint torque sensor is inserted. The introduction of a time-varying stability factor enhances the performance of the RLS scheme so as to handle also poor excitation conditions, e.g. due to the smaller deformations of the transmission typical of serial VSAs, optimizing the convergence rate and preventing drift of the estimated model parameters.

As a further merit, being the proposed approach designed on the motor side of the flexible transmissions, it is straightforward to address the stiffness estimation problem in a decentralized way for the case of multi-DOF VSA-driven robots, without noticeable differences caused by the additional dynamic couplings.

Extensive simulations conducted under realistic conditions on representative devices of the considered VSA categories, the antagonistic VSA-II, the serial AwAS, as well as for a multi-DOF case, have illustrated the robust properties of the method with respect to noise and discretization of measurements. The experimental results obtained on the AwAS platform have validated the approach and shown a good performance of the stiffness estimation method.

From the control point of view, the proposed estimator has several advantages. The online nature of the estimation allows its insertion in regulation or tracking control schemes, using the time-varying estimate of the stiffness as feedback signal. The parametric model representation allows stiffness derivatives to be obtained in closed analytic form. This is important when implementing a feedback linearization control law or a global regulator with exact cancellation of the non-collocated gravity term. The proof of closed-loop stability related to estimation-based control laws is challenging, in view of the nonlinearity of

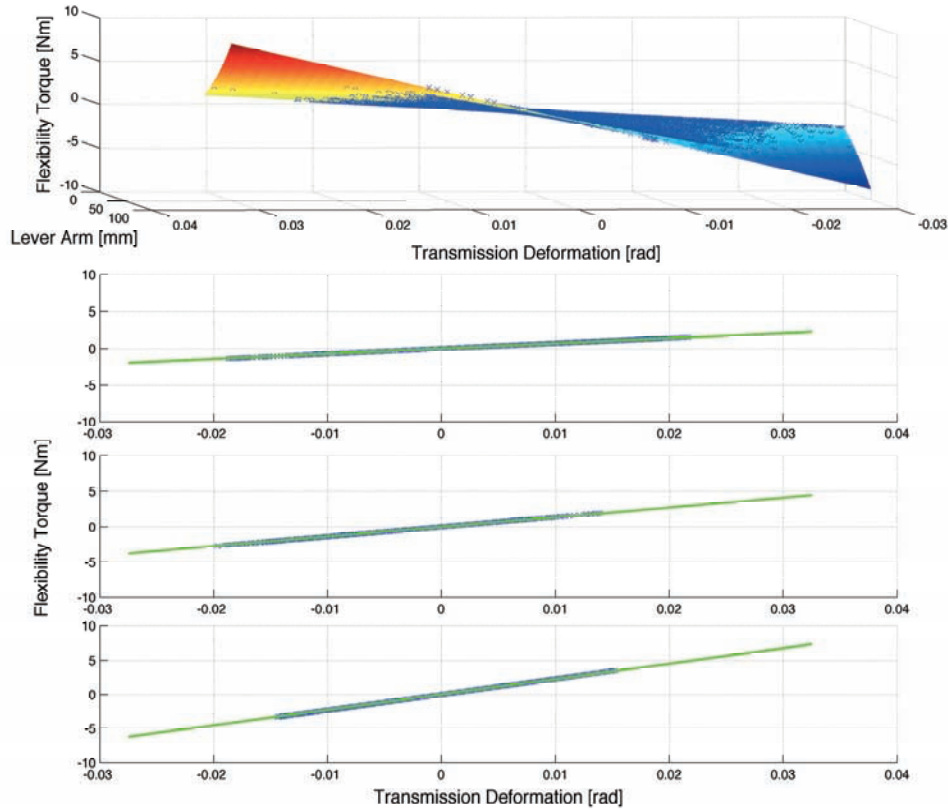


Fig. 32. Characteristic surface of the flexibility torque as a function of the transmission deformation ϕ and the lever arm r obtained with the final estimated polynomial parameters, with superposed data collected during the experiment (crosses, blue). The other three plots represent slices of the flexibility torque characteristic at fixed lever arm lengths $r = 50, 70, 90$ [mm].

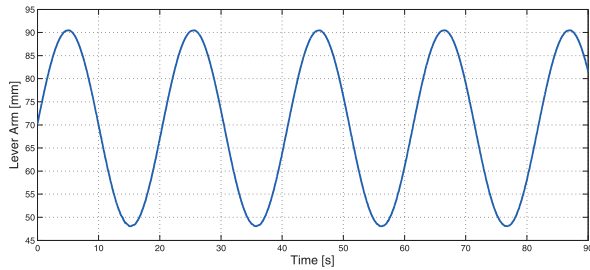


Fig. 33. Lever arm length r in the AwAS validation experiment.

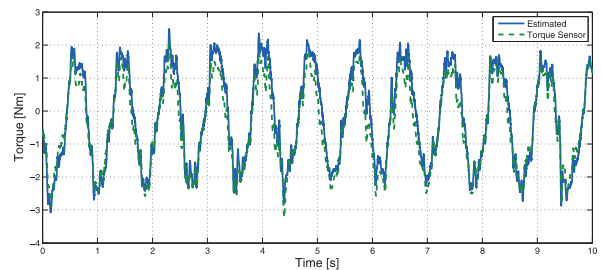


Fig. 35. Flexibility torque in the AwAS validation experiment: previously estimated model (solid, blue) and measured by the torque sensor (dashed, green); expanded view for 10 s.

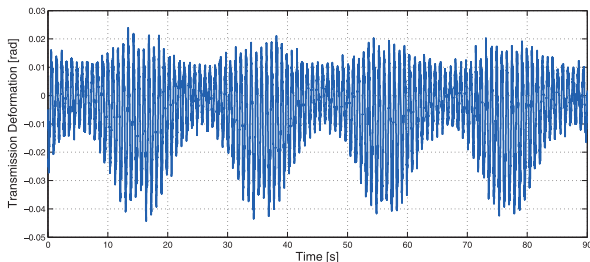


Fig. 34. Transmission deformation ϕ in the AwAS validation experiment.

the problem and the lack of a separation principle. However, preliminary results of Flacco and De Luca (2011b), where the stiffness estimator was combined with a nonlinear decoupling control for the VSA-II, show the practical feasibility.

An experimental validation of a feedback controller for the AwAS that uses the stiffness estimated online with the proposed approach is part of our future plans. An interesting extension of this work includes an adaptive version of the estimator to cope with large uncertainties in the motor inertia and damping parameters. Further, the development of an even more robust version of the RLS algorithm,

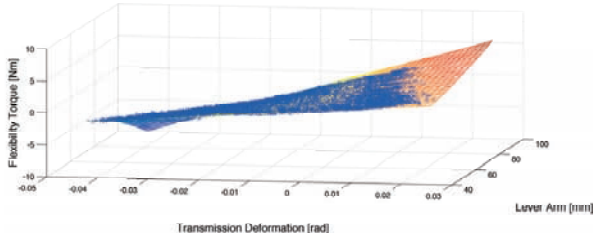


Fig. 36. Characteristic surface of the flexibility torque as a function of the transmission deformation ϕ and the lever arm r obtained with the AwAS stiffness model estimated at the end of the first experiment, superposed to the data collected during a second validation experiment (crosses, blue).

based on orthogonal factorizations of the covariance matrix, would be able to prevent the loss of symmetry and convergence issues related to strongly ill-conditioned estimation problems.

Notes

1. We gladly acknowledge the seminal discussion on this problem between the second author and Professor Antonio Bicchi, during the return flight from the IROS'09 conference held in Kobe.
2. This idea was introduced independently also by Flacco and De Luca (2011a) and is reprised in the present paper.
3. As is customary, we model a flexible geared transmission as a rigid and loss-less reduction gear followed in series by a flexible element.
4. This situation is typically associated with a steady state where no external torques act on the transmission. If in this situation the transmission deformation is $\dot{\phi} = 0$ because of a specific mechanical implementation or due to an imposed pretension, we can still satisfy assumption (1) by applying an offset to the measurements, i.e. $\phi = \phi_{measured} - \bar{\phi}$.
5. Some of the existing electrically driven VSA designs do not fit directly in the model formats of Sections 2.2 or 2.3. One example is the VSA-I proposed by Tonietti et al. (2005), due to the presence of an extra elastic coupling between the two driving motors.
6. The correctness of these data depends on the quality of the motor. In case of inaccurate values, an offline identification of these parameters is needed.
7. Other choices of basis functions can be made, e.g. Fourier approximations. A polynomial basis is computationally simple and has given good results in all considered cases.
8. This practical condition of sufficient excitation is only in part related to the concept of persistent excitation for the identification of linear dynamic systems.

Funding

This work was supported by the European Commission (grant numbers FP7-ICT-2011 287513 SAPHARI and FP7-ICT-2007 231554 VIATORS).

References

Bicchi A, Bavaro M, Boccadamo G, et al. (2008a) Physical human–robot interaction: dependability, safety, and performance. In *Proceedings 10th International Workshop on Advanced Motion Control*, pp. 9–14.

- Bicchi A, Peshkin MA and Colgate JE (2008b) Safety for physical human–robot interaction. In Siciliano B and Khatib O (eds), *Springer Handbook of Robotics*. New York: Springer, pp. 1335–1348.
- Bicchi A and Tonietti G (2004) Fast and soft arm tactics: Dealing with the safety–performance trade-off in robot arms design and control. *IEEE Robotics and Automation Magazine* 11(2): 22–33.
- Bittanti S, Bolzern P and Campi M (1990) Recursive least-squares identification algorithms with incomplete excitation: Convergence analysis and application to adaptive control. *IEEE Transactions on Automatic Control* 35: 1371–1373.
- Choi J, Park S, Lee W and Kang S-C (2008) Design of a robot joint with variable stiffness. In *Proceedings IEEE International Conference on Robotics and Automation*, pp. 1760–1765.
- Coutinho F and Cortesao R (2010) System stiffness estimation with the candidate observers algorithm. In *Proceedings 18th Mediterranean Conference on Control and Automation*, pp. 796–801.
- De Luca A, Albu-Schäffer A, Haddadin S and Hirzinger G (2006) Collision detection and safe reaction with the DLR-III lightweight robot arm. In *Proceedings IEEE/RSJ International Conference on Intelligent Robots and Systems*, pp. 1623–1630.
- De Luca A and Book W (2008) Robots with flexible elements. In Siciliano B and Khatib O (eds), *Springer Handbook of Robotics*. New York: Springer, pp. 287–319.
- De Luca A and Flacco F (2010) Dynamic gravity cancellation in robots with flexible transmissions. In *Proceedings 49th IEEE Conference on Decision and Control*, pp. 288–295.
- De Luca A, Flacco F, Bicchi A and Schiavi R (2009) Non-linear decoupled motion–stiffness control and collision detection/reaction for the VSA-II variable stiffness device. In *Proceedings IEEE/RSJ International Conference on Intelligent Robots and Systems*, pp. 5487–5494.
- De Luca A and Lucibello P (1998) A general algorithm for dynamic feedback linearization of robots with elastic joints. In *Proceedings IEEE International Conference on Robotics and Automation*, pp. 504–510.
- De Luca A and Mattone R (2003) Actuator failure detection and isolation using generalized momenta. In *Proceedings IEEE International Conference on Robotics and Automation*, pp. 634–639.
- De Luca A, Siciliano B and Zollo L (2005) PD control with on-line gravity compensation for robots with elastic joints: Theory and experiments. *Automatica* 41: 1809–1819.
- De Santis A, Siciliano B, De Luca A and Bicchi A (2008) An atlas of physical human–robot interaction. *Mechanism and Machine Theory* 43: 253–270.
- Diolaiti N, Melchiorri C and Stramigioli S (2005) Contact impedance estimation for robotic systems. *IEEE Transactions on Robotics* 21: 925–935.
- Flacco F and De Luca A (2011a) Residual-based stiffness estimation in robots with flexible transmissions. In *Proceedings IEEE International Conference on Robotics and Automation*, pp. 5541–5547.
- Flacco F and De Luca A (2011b) Stiffness estimation and nonlinear control of robots with variable stiffness actuation. In *18th IFAC World Congress*, pp. 6872–6879.
- Flacco F, De Luca A, Sardellitti I and Tsagarakis NG (2011) Robust estimation of variable stiffness in flexible joints. In

- Proceedings IEEE/RSJ International Conference on Intelligent Robots and Systems*, pp. 4026–4033.
- Garabini M, Passaglia A, Belo F, Salaris P and Bicchi A (2011) Optimality principles in variable stiffness control: The VSA hammer. In *Proceedings IEEE/RSJ International Conference on Intelligent Robots and Systems*, pp. 3770–3775.
- Grioli G and Bicchi A (2010) A non-invasive real-time method for measuring variable stiffness. In *Proceedings Conference Robotics: Science and Systems (RSS 2010)*, Zaragoza, Spain.
- Grioli G and Bicchi A (2011) A real-time parametric stiffness observer for VSA devices. In *Proceedings IEEE International Conference on Robotics and Automation*, Shanghai, China.
- Haddadin S, Albu-Schäffer A, De Luca A and Hirzinger G (2007) Safety evaluation of physical human–robot interaction via crash-testing. In *Proceedings Conference on Robotics: Science and Systems (RSS 2007)*, Atlanta, GA.
- Haddadin S, Laue T, Frese U, Wolf S, Albu-Schäffer A and Hirzinger G (2009) Kick it with elasticity: Safety and performance in human robot soccer. *Robotics and Autonomous Systems* 57: 761–775.
- Hirzinger G, Albu-Schäffer A, Hähle M, Schaefer I and Sporer N (2001) On a new generation of torque controlled lightweight robots. In *Proceedings IEEE International Conference on Robotics and Automation*, pp. 3356–3363.
- Ikegami Y, Nagai K, Loureiro R and Harwin W (2009) Design of redundant drive joint with adjustable stiffness and damping mechanism to improve joint admittance. In *Proceedings IEEE International Conference on Rehabilitation Robotics*, pp. 202–210.
- Ikuta K, Ishii H and Nokata M (2003) Safety evaluation method of design and control for human-care robots. *The International Journal of Robotics Research* 22: 281–297.
- Jafari A, Tsagarakis N, Vanderborght B and Caldwell D (2010) A novel actuator with adjustable stiffness (AwAS). In *Proceedings IEEE/RSJ International Conference on Intelligent Robots and Systems*, pp. 4201–4206.
- Jeon S and Tomizuka M (2007) Benefits of acceleration measurements in velocity estimation and motion control. *IFAC Control Engineering Practice* 15: 325–332.
- Johnson C (1988) *Lectures on Adaptive Parameter Estimation*. Englewood Cliffs, NJ: Prentice Hall.
- Kugi A, Ott C, Albu-Schäffer A and Hirzinger G (2008) On the passivity-based impedance control of flexible joint robots. *IEEE Transactions on Robotics* 24: 416–429.
- Ludvig D and Kearney RE (2009) Estimation of joint stiffness with a compliant load. In *Proceedings 31st IEEE International Conference on EMBS*, pp. 2967–2970.
- Migliore S, Brown E and DeWeerth S (2005) Biologically inspired joint stiffness control. In *Proceedings IEEE International Conference on Robotics and Automation*, pp. 4508–4513.
- Ozawa R and Kobayashi H (2002) Response characteristics of elastic joint robots driven by various types of controllers against external disturbances. In *Proceedings 6th International Conference on Motion and Vibration Control*, pp. 420–425.
- Palli G, Melchiorri C and De Luca A (2008) On the feedback linearization of robots with variable joint stiffness. In *Proceedings IEEE International Conference on Robotics and Automation*, pp. 1753–1759.
- Petit F and Albu-Schäffer A (2011) Cartesian impedance control for a variable stiffness robot arm. In *Proceedings IEEE/RSJ International Conference on Intelligent Robots and Systems*, pp. 4180–4186.
- Pratt GA and Williamson MM (1995) Series elastic actuators. In *Proceedings IEEE/RSJ International Conference on Intelligent Robots and Systems*, pp. 399–406.
- Salisbury K, Townsend W, Eberman B and DiPietro D (1988) Preliminary design of whole-arm manipulation systems (WAMS). In *Proceedings IEEE International Conference on Robotics and Automation*, pp. 254–260.
- Sardellitti I, Medrano-Cerda G, Tsagarakis N, Jafari A and Caldwell D (2012) A position and stiffness control strategy for variable stiffness actuators. *Proceedings IEEE International Conference on Robotics and Automation* pp. 2785–2791.
- Schiavi R, Grioli G, Sen S and Bicchi A (2008) VSA-II: A novel prototype of variable stiffness actuator for safe and performing robots interacting with humans. In *Proceedings IEEE International Conference on Robotics and Automation*, pp. 2171–2176.
- Serio A, Grioli G, Sardellitti I, Tsagarakis NG and Bicchi A (2011) A decoupled impedance observer for a variable stiffness robot. In *Proceedings IEEE International Conference on Robotics and Automation*, pp. 5548–5553.
- Spong MW (1987) Modeling and control of elastic joint robots. *ASME Journal of Dynamic Systems, Measurement, and Control* 109: 310–319.
- Tonietti G, Schiavi R and Bicchi A (2005) Design and control of a variable stiffness actuator for safe and fast physical human/robot interaction. In *Proceedings IEEE International Conference on Robotics and Automation*, pp. 528–533.
- Tsagarakis N, Sardellitti I and Caldwell D (2011) A new variable stiffness actuator (CompAct-VSA): Design and modelling. In *Proceedings IEEE/RSJ International Conference on Intelligent Robots and Systems*, pp. 378–383.
- Van Ham R, Sugar T, Vanderborght B, Hollander K and Lefeber D (2009) Compliant actuator designs. *IEEE Robotics and Automation Magazine* 16(3): 81–94.
- Van Ham R, Vanderborght B, Van Damme M, Verrelst B and Lefeber D (2007) MACCEPA, the mechanically adjustable compliance and controllable equilibrium position actuator: Design and implementation in a biped robot. *Robotics and Autonomous Systems* 10: 761–768.
- Verscheure D, Scharf I, Bruyninckx H, Swevers J and De Schutter J (2009) Identification of contact dynamics parameters for stiff robotic payloads. *IEEE Transactions on Robotics* 25: 240–252.
- Visser L, Carloni R and Stramigioli S (2011) Energy-efficient variable stiffness actuators. *IEEE Transactions on Robotics* 27: 865–875.
- Wolf S and Hirzinger G (2008) A new variable stiffness design: Matching requirements of the next robot generation. In *Proceedings IEEE International Conference on Robotics and Automation*, pp. 1741–1746.